

# Multi-Set Space-Time Shift Keying And Space-Frequency Space-Time Shift Keying for Millimeter-Wave Communications

Ibrahim A. Hemadeh, *Student Member, IEEE*, Mohammed El-Hajjar, *Senior Member, IEEE*, SeungHwan Won, *Senior Member, IEEE*, and Lajos Hanzo, *Fellow, IEEE*

**Abstract**—In this paper, we introduce a novel OFDM-aided multi-functional multiple-input multiple-output (MIMO) scheme based on Multi-Set Space-Time Shift Keying (MS-STSK), where the information transmitted over each sub-carrier is divided into two parts, namely the STSK codeword and the implicit antenna combination (AC) index. In MS-STSK, a unique combination of antennas can be activated at each sub-carrier in order to convey extra information over the AC index, while additionally transmitting the STSK codeword. Furthermore, inspired by the MS-STSK concept, this scheme is additionally extended also to the frequency domain in the novel context of our Multi-Space-Frequency STSK (MSF-STSK), where the total number of sub-carriers is partitioned into blocks in order to implicitly carry the block's frequency index. The proposed MSF-STSK scheme benefits from the huge bandwidths available at mmWaves for partitioning the total number of OFDM sub-carriers into blocks in order to convey more information over the frequency domain. Both proposed systems use STSK codewords as the basic transmission block and they can achieve higher data throughput and better BER performance than STSK. Moreover, given that the system is meant to operate at mmWaves, antenna arrays relying on several antenna elements are employed at both the transmitter and receiver for analogue beamforming (ABF) with the aid of phase shifters and power amplifiers for the sake of overcoming the effect of high path loss.

**Index Terms**—Millimeter Waves, wideband channel, MIMO, Space-Time Shift Keying, Spatial Modulation, PSK, QAM.

## I. INTRODUCTION

Millimeter wave (mmWave) communications constitutes a promising technique for next-generation wireless communications systems [1], [2]. Due to their huge available bandwidths, mmWaves have been attracting considerable attention with a view to replace or to collectively operate with the saturating sub-3 GHz band [3]. However, as a predicament, mmWaves suffer from high attenuation [4], which fortunately can be mitigated with the aid of accommodating large antenna arrays within relatively small areas for the sake of attaining array gains [5]. As a result for mmWaves, beamforming is considered to be the most suitable multiple-input multiple-output (MIMO) technique.

The financial support of the EPSRC projects EP/N004558/1 and EP/L018659/1, as well as of the European Research Council's Advanced Fellow Grant under the Beam-Me-Up project and of the Royal Society's Wolfson Research Merit Award is gratefully acknowledged.

The family of MIMO schemes devised for wireless communications systems shown in Figure 1 is capable of achieving enhanced transmission rates and an improved communication integrity [6]. For instance, multiplexing techniques, such as the Bell-Labs Layered Space-Time (BLAST) [7] laying under the multiplexing branch of MIMO techniques in Figure 1 are capable of attaining enhanced transmission rates. By contrast, the diversity-oriented MIMO techniques shown in Figure 1, such as Orthogonal Space-Time Block Coding (OSTBC) [8] and its STBC extensions [9] as well as the Space Time Trellis Code (STTC) [10] would achieve diversity gains. Furthermore, Spatial Modulation (SM) [11], [12], [13] is capable of achieving both diversity and multiplexing gains by conveying extra information over the activated transmit antenna index. This scheme was employed successfully for transmission over mmWaves in a Line-of-Sight (LOS) environment [14].

Furthermore, combining two or more MIMO techniques would result in a generalized MIMO scheme referred to as the Multi-Functional (MF) MIMO scheme [15]. MF-MIMOs can be employed for communications over mmWaves, since they are capable of combining the benefits of different MIMO schemes, which is essential for overcoming the high mmWaves attenuation by employing beamforming, whilst simultaneously achieving performance and/or throughput enhancements using diversity and/or multiplexing techniques. An example of MF-MIMOs is constituted by the Layered Steered Space-Time Coding (LSSTC) concept [16], which is capable of achieving a multiplexing gain, diversity gain and Signal-to-Noise (SNR) gain by combining V-BLAST, STBC and Analogue Beamforming (ABF). Another MF-MIMO is the popular Space-Time Shift Keying (STSK) scheme, which was proposed in [17] as a generalized MIMO relative of SM that combines it with Linear Dispersion Codes (LDC) as shown in Figure 1, where instead of activating a single transmit antenna, a single dispersion matrix is activated. This scheme is capable of achieving both multiplexing and diversity gains, whilst striking a compelling trade-off between them. Furthermore, in [18] we proposed an extended STSK referred to as Multi-Set (MS) STSK, where -in addition to the explicit information carried by the STSK codeword- extra information is conveyed implicitly over the index of the activated combination of multiple antennas selected from a higher number of antenna elements.

In [19], we proposed an STSK-based mmWave system for Multi-User (MU) downlink (DL) scenarios. The system con-

ABF	Analogue Beamforming	MIMO	Multiple-Input Multiple-Output
AC	Antenna Combination	ML	Maximum Likelihood
AE	Antenna Elements	mmWave	Millimeter Wave
ASU	Antenna Selection Unit	MSF	Multi-Space-Frequency
AWGN	Additive White Gaussian Noise	MS-STSK	Multi-Set Space-Time Shift Keying
BER	Bit Error Rate	MU	Multi-User
BLAST	Bell-Labs Layered Space-Time	OFDM	Orthogonal Frequency-Division Multiplexing
BPC	Bits Per Codeword	OSTBC	Orthogonal STBC
BPC	Bits Per Symbol	PSK	Phase-Shift Keying
CP	Cyclic Prefix	QAM	Quadrature Amplitude Modulation
CSI	Channel State Information	RAA	Receive Antenna Array
DAC	Distinct AC	RAE	Receive Antenna Element
FI	Frequency Index	SAC	Shared AC
GSFIM	Generalized Space-Frequency Index Modulation	SSK	Space-Shift Keying
GSIM	Generalized Spatial Index Modulation	ST	Space-Time
HL	Hard-Limiter	STBC	Space-Time Block Code
ICI	Inter-Channel Interference	STSK	Space-Time Shift Keying
LDC	Linear Dispersion Coding	SM	Spatial Modulation
LSSTC	Layered Steered Space-Time Coding	SNR	Signal-to-Noise Ratio
MF	Multi-Functional	TAA	Transmit Antenna Array
		TAE	Transmit Antenna Element
		MU-TPC	MU-Transmit Precoding

Table I  
NOMENCLATURE

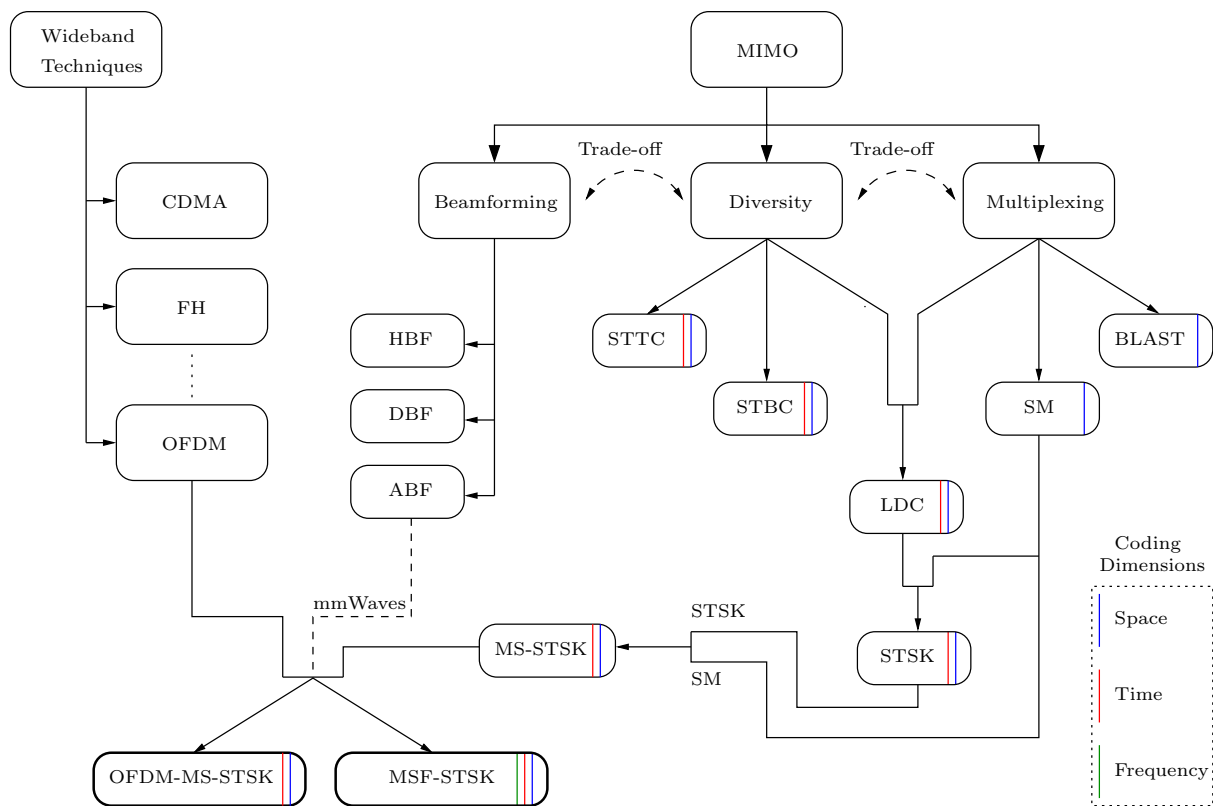


Figure 1. Family tree of MS-STSK, OFDM-MS-STSK and MSF-STSK.

$N_{RF}^t$	Number of transmitter RF chains	$r_{n_r, T_i}$	The signal received at the output of the $n_r$ -th receive AE at the $T_i$ MS-STSK time slot
$N_t$	Number of transmitter antennas		
$N_{RF}^r$	Number of receiver RF chains	$h_{n_r, n_t}$	Or $h_{n_r, n_t}(t, \tau, \theta, \varphi)$ : double-directional CIR
$N_r$	Number of receiver antennas		
$\theta_{AC}$	Phase shift rotation	$N_{sc}$	Number of sub-carriers, where $n_{sc} = 1, \dots, N_{sc}$
$\Delta\theta$	Phase-shift difference between two ACs	$N_{cp}$	CP length
$\mathcal{O}(\cdot)$	Complexity order	$\mathcal{F}_{T_i}$	The $T_i$ -th OFDM symbol
$M_Q$	Number of dispersion matrices, where $q = 1, \dots, M_Q$	$\mathbf{R}_{T_i}(n_{sc})$	The signal received at the $n_{sc}$ -th sub-carrier within the $T_i$ -th MS-STSK slot
$M_c$	Constellation size, where $l = 1, \dots, M_c$	$\mathbf{W}(n_{sc})$	ABF precoder at the $n_{sc}$ -th sub-carrier
$N_{AC}$	Number of combinations, where $n_{AC} = 1, \dots, N_{AC}$	$\mathbf{Z}(n_{sc})$	ABF combiner at the $n_{sc}$ -th sub-carrier
		$\mathbf{R}$	The $n_{sc}$ -th received MS-STSK symbol
$N_B$	Size of the sub-carriers block, where $n_B = 1, \dots, N_B$	$\hat{\mathbf{H}}(n_{sc})$	The frequency domain of the discrete-time CIR
$N_{FI}$	The number of ACs dedicated to FI encoding, where $n_{FI} = 1, \dots, N_{FI}$	$\mathbf{H}$	Effective channel observed after applying the transmit and receive ABF
		$\bar{\mathbf{R}}$	Vectorized received signal
$T$	Number of STSK time slots, where $T_i = 1, \dots, T$	$\bar{\mathbf{H}}$	Vectorized equivalent channel
		$\mathbf{H}_c$	Activated combination effective channel
$M$	Number of STSK spaces, where $m = 1, \dots, M$	$\mathbf{h}_{c,q}$	The $q$ -th column of the $c$ -th effective channel $\mathbf{H}_c$
$B_{ASU}$	Number of bits fed into the ASU	$\mathcal{X}$	Vectorized MS-STSK dispersion matrices
$B_{STSK}$	Number of bits fed into the STSK encoder	$\mathcal{I}$	AC activation matrix
		$\mathbf{I}_C$	Identity matrix at the $c$ -th position in $\mathcal{I}$
$B_{MS-STSK}$	Number of MS-STSK encoded bits	$\mathbf{K}$	QAM/PSK symbol activation vector
		$\Delta\theta_c$	Phase-shift difference between two ACs
$B_{FI}$	Number of bits used for the FI	$\hat{\mathbf{y}}_{c,q}$	Equalized received signal by the $c$ -th channel combination and the $q$ -th dispersion matrix
$\tilde{\mathbf{X}}$	STSK codeword		
$\mathbf{X}$	MS-STSK codeword		
$\tilde{A}_{q, n_{AC}}$	MS-STSK dispersion matrix	$\hat{s}_l$	The estimate of the $l$ -th transmitted symbol
$s_l$	QAM/PSK symbol		

Table II  
LIST OF SYMBOLS.

sidered a wideband mmWave channel, where Orthogonal Frequency Division Multiplexing (OFDM) combined with a digital-analogue hybrid structure is employed for overcoming the effect of the time dispersive multipath channel with the aid of a linear MU-Transmit precoding (MU-TPC) technique used for MU access. Transmitting over wideband channels requires wideband channel techniques, such as Code Division Multiple Access (CDMA), Frequency Hopping (FH) and OFDM [6], as shown in Figure 1. Furthermore, using the aforementioned hybrid architecture is essential for mmWave systems [20], where the digital part provides a high design flexibility in

terms of signal processing [21], while the analogue part is capable of compensating for having a reduced number of RF chains by providing high array gains with the aid of large antenna arrays [22]. Hybrid system arrangements are capable of striking an attractive design trade-off between the system performance and the power consumption of high-frequency system components [23].

*In this paper, we propose a pair of system designs for mmWaves, where the digital precoding part of the preferably hybrid beamforming required for increasing the number of data streams transmitted is replaced by applying MIMO*

signal processing techniques. The first is a novel realization of MS-STSK combined with OFDM for communication over mmWaves referred to as the OFDM-MS-STSK scheme shown in Figure 1. This space-time subsidized system is capable of striking a trade-off between the achievable throughput and the diversity gains attained, which subsumes the SM [11], STSK [17], and Space-Shift Keying (SSK) [24] schemes as special cases. Using OFDM, the huge mmWave channel bandwidth is partitioned into a high number of narrow sub-bands, where an antenna combination (AC) is activated at each sub-carrier to transmit an STSK codeword, hence implicitly transmitting extra information over the activated antenna combination index in addition to the explicit STSK coded bits. The concept of sub-carrier indexing was utilized in the OFDM Index Modulation (OFDM-IM) scheme [25] for improving the achievable throughput, where extra information is conveyed over the sub-carrier index. This work was later extended both in [26] by introducing an alternative sub-carrier grouping technique, and in [27] by advocating a low-complexity optimal detection technique. Furthermore, in [28] the minimum distance of the classic constellation and index-constellation was jointly optimized. Finally, the achievable performance was further improved with the aid of compressed sensing in [29].

Furthermore, this work is extended to additionally exploit the frequency dimension. The work in [30] applied frequency indexing by transmitting modulated symbols in a unique block pattern. Furthermore, the STSK concept was extended both to Space-Frequency Shift Keying (SFSK) and to Space-Time-Frequency Shift Keying (STFSK) schemes in [31], where the transmitted information is collectively spread over the space, time and frequency domains.

In our second proposed scheme, we present an extended version of the OFDM-MS-STSK technique, where the frequency index is exploited for the sake of implicitly conveying extra information, with the total number of sub-carriers being partitioned into blocks of sub-carriers and the frequency index of the block is expressed by a unique antenna combination activated at a specific sub-carrier. This system is referred to as the Multi-Space-Frequency (MSF) STSK scheme is shown in Figure 1. Both the proposed systems are combined with analogue beamforming for the sake of mitigating the effect of the high attenuations of mmWaves. As a benefit of the huge available mmWave bandwidth, the channel can be partitioned into a large number of sub-carriers, which can benefit the system in terms of many aspects. More specifically, increasing the number of sub-carriers would increase the normalized throughput of both proposed systems by reducing the normalized overhead of the long Cyclic Prefix (CP) required at mmWaves [32], [19]. Furthermore, as a benefit of reducing the number of sub-carriers the number of frequency partitions increases, which thereby implies that the extra information conveyed by frequency indexing further increases.

The novel contributions of this paper can be summarized as follows:

- We intrinsically amalgamate the MS-STSK scheme both with OFDM in order to operate over the wideband mmWave channel as well as with beamforming for over-

coming the high path loss of the mmWave channel.

- We propose the MSF-STSK concept, where the transmit information is spread over the space-time-and frequency-domains. Hence, additional throughput enhancements may be gleaned from beneficially combining the three domains.

This paper is organized as follows. In Section II, we present the OFDM-MS-STSK system proposed for mmWave communications. Then in Section III, we introduce the extended frequency-domain version of MS-STSK referred to as the MSF-STSK system. Finally, we conclude in Section IV.

**Notations:** Bold upper case letters represent matrices;  $\lfloor \cdot \rfloor$  denotes the flooring of a real number to the nearest smallest following integer, while  $\lceil \cdot \rceil$  denotes the rounding operation of a real number to the nearest integer;  $\text{mod}(\cdot)$  indicates the modulus operation;  $\binom{n}{r}$  denotes the combinations without repetition of  $n$  objects taken  $r$  at a time;  $()^T$  represents the transpose operation and  $(\cdot)^H$  represents the Hermitian transpose operation;  $\mathbb{C}^{a \times b}$  indicates a matrix of complex numbers of the size  $a \times b$ ;  $\|\cdot\|$  denotes the Frobenius norm and  $|\cdot|$  indicates the modulus of a complex number; The  $\otimes$  operator denotes the circular convolution operation.

## II. MULTI-SET SPACE-TIME SHIFT KEYING SYSTEM FOR MMWAVES

In this section, we intrinsically amalgamate the novel MS-STSK scheme proposed in [18] both with ABF and OFDM for transmission over the mmWave channel. The MS-STSK scheme is an SM-MIMO scheme, where as shown in Figure 2, instead of activating a single transmit antenna in order to implicitly convey the antenna index, a unique, data-specific combination of transmit antennas is activated for transmitting an STSK codeword [17], [33]. STSK is a flexible scheme, where the codewords generated can be flexibly tuned, which could fit any arbitrary transmit antenna size, while striking a trade-off between the achievable diversity gain and the attainable throughput. Different antenna combinations are shown in Figure 2 as a distinct set of multiple antennas. The transmit antennas are spaced far enough to experience independent fading, where the ones activated can be viewed as a distinct set of multiple antennas. The MS-STSK system conveys information over both the STSK codeword and the transmit Antenna Combination (AC) index. An AC is defined as a combination of multiple transmit antennas that are activated to transmit a single STSK codeword.

In order to formulate a symbol set, the number of combinations should ideally be a power of two. This may be achieved either by having a distinct set of AEs for each AC, or with the aid of a distinct combination of AEs out of the total number of available AEs. In the light of this principle, the pair of AC allocation techniques shown in Figure 3 were proposed in [18]. The antenna allocation technique shown in Figure 3(a) is referred to as the Shared Antenna Allocation (SAC) technique, where one or more antenna elements can be shared by several ACs. By contrast, the technique shown in Figure

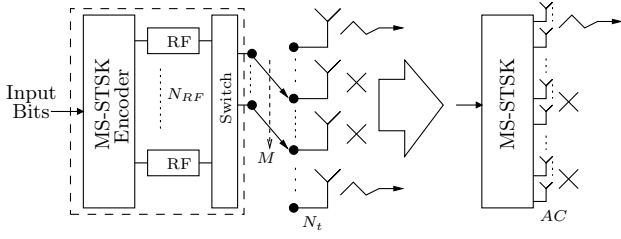


Figure 2. The MS-STSK transmitter block diagram viewed as an SM-MIMO.

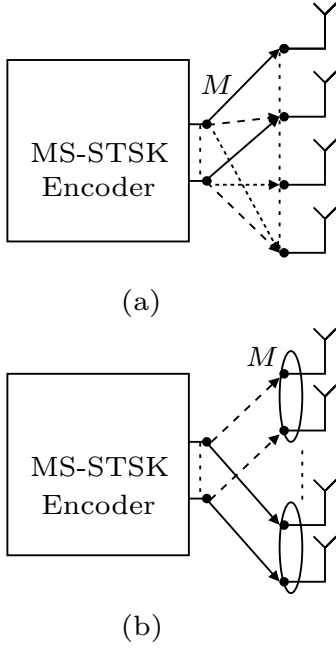


Figure 3. MS-STSK block diagram associated (a) with ACs with shared AEs (b) with ACs with distinct sets of AEs.

3(b) is referred to as the Distinct Antenna Allocation (DAC) technique, where  $M$  unique AEs are assigned to each AC, i.e. No AEs are shared by the ACs. Furthermore, the general structure of the MS-STSK transmitter is shown in Figure 2, where regardless of the AC allocation technique employed, the MS-STSK transmission mechanism can be characterized by activating one of  $N_{AC}$  antenna sets, each formed of  $M$  AEs.

Owing to the time dispersive and frequency selective nature of mmWave wideband channels [34], [35], [36], wideband techniques such as OFDM and SC-FDE have to be used for communication over the mmWave channel for the sake of mitigating the ISI imposed by the channel. In this study, we employ the OFDM scheme, which subdivides the wideband channel into a large number of orthogonal narrow-band sub-carriers. Together with MS-STSK, extra information carried over the activated AC index may be transmitted over each OFDM sub-carrier with the aid of an MS-STSK encoder, which can be used for mapping each STSK codeword at each sub-carrier to its corresponding transmit antenna combination. The amalgamated system combination of OFDM and MS-STSK is referred to as OFDM-MS-STSK and in what follows it is invoked for NLOS mmWave scenarios.

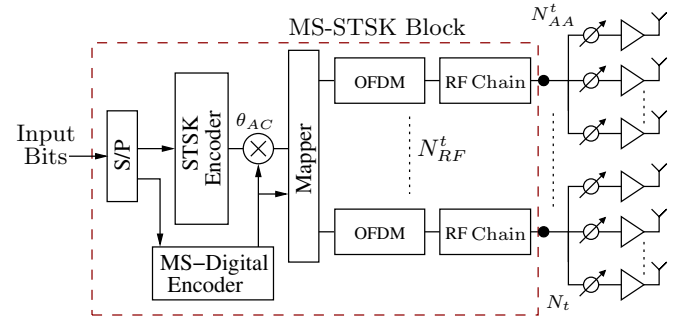


Figure 4. Transmitter block diagram of the OFDM-MS-STSK system.

The OFDM-aided MS-STSK transmitter referred to as OFDM-MS-STSK is equipped with  $N_{RF}^t$  Transmit Antenna Arrays (TAAs) for the sake of achieving analogue beamforming, which is a key enabling technology for mmWave systems relying on a pair of phase-shifters and power amplifiers dedicated to each of the Transmit Antenna Elements (TAEs)<sup>1</sup>. Similarly, the receiver is equipped with  $N_{RF}^r$  Receive Antenna Arrays (RAAs) for the sake of achieving further beamforming gain.

#### A. OFDM-MS-STSK Transmitter

Consider the OFDM-MS-STSK transmitter shown in Figure 4 equipped with  $N_{RF}^t$  TAAs and a total of  $N_t$  TAEs, where each TAA consists of  $N_{AA}^t$  antenna array elements for the sake of applying ABF with the aid of a pair of phase-shifters and power amplifiers. The  $N_{RF}^t$  RF chains comprise all the components needed for baseband to RF up-conversion, including the digital-to-analogue converter, up-conversion, filters, power amplifiers (PA) and low noise amplifiers (LNA) [37]. Hence, reducing the required number of RF chains is desirable for reducing the transmitter's cost. The MS-STSK encoder is fed with a block of  $B_{MS-STSK}$  bits, which divides the input bits into  $B_{STSK}$  and  $B_{ASU}$  bits with the aid of the serial-to-parallel (S/P) converter shown in Figure 4 in order to feed the STSK encoder and multi-set (MS) precoder with their corresponding bit streams.

The STSK encoder generates the STSK codeword  $\tilde{\mathbf{X}}$  by spreading the  $B_{STSK} = \log_2(M_c M_Q)$  number of input bits over  $T$  time intervals and  $M$  spatial dimensions, where  $M_c$  is the QAM/PSK constellation size and  $M_Q$  is the total number of dispersion matrices. The STSK codeword is expressed as

$$\tilde{\mathbf{X}} = A_q s_l, \quad (1)$$

where  $s_l$  is the  $M_c$ -PSK/QAM symbol and  $A_q \in \mathbb{C}^{M \times T}$  is the activated dispersion matrix of the dispersion matrix set  $\{A_q\}_{q=1}^{M_Q}$ . The dispersion matrices are generated based on the random search process described in [33] satisfying the power constraint of  $\text{tr}(A_q^H A_q) = T$  for  $q = 1, \dots, M_Q$ .

As shown in Figure 4, the S/P converter located at the transmitter's input provides the MS-Digital precoder with  $B_{AS}$  bits used for mapping the STSK codeword to its corresponding

<sup>1</sup>Transmit antenna arrays contain multiple AEs used to apply ABF.

transmit AC. Based on a bit-to-AC look-up table [18], the MS encoder applies a phase-shift of  $\theta_{AC}$  to the modulated symbol  $s_l$  and maps the STSK codeword to its appropriate AC, regardless of the AC allocation technique employed, where a zero phase-shift is applied for MS-STSK encoding associated with the DAC.

The total number of ACs in the classical MS-STSK scheme presented in [18] relies on both the total number of AEs and the size of  $M$ . By contrast, the total number of ACs in the OFDM-MS-STSK scheme is jointly determined by the total number of TAAs and the size of  $M$ , since each TAA of size  $N_{RF}^t$  AEs carries a single stream, while in the classical MS-STSK scheme the streams are transmitted by each TAE. Hence, the total number of encoded bits characterizing the AC indices can be expressed as

$$B_{ASU} = \left\lceil \log_2 \left( \frac{N_{RF}^t}{M} \right) \right\rceil, \quad (2)$$

for OFDM-MS-STSK associated with SAC and as

$$B_{ASU} = \log_2 \left( \frac{N_{RF}^t}{M} \right), \quad (3)$$

for OFDM-MS-STSK associated with DAC.

The SAC technique represents the general AC allocation technique of MS-STSK, which includes the DAC technique as a special case [18]. Hence, we consider it as the main AC allocation technique for the sake of reducing the total number of RF chains required for achieving a specific throughput. The DAC technique would require a higher number of TAAs than the SAC to achieve a specific throughput, which would impose an increased terminal cost as a result of the increased number of RF chains.

When the same TAA participates in multiple ACs, an inter-dependence is introduced between them [18], [38], hence a phase shift  $\theta_{n_{AC}}$  is applied to each STSK codeword in order to overcome the correlation introduced by the common TAAs in different ACs. In MS-STSK [18], each AC is given a predefined phase-shift based on the modulation scheme adopted. The phase shift mainly rotates the symbol constellation used, hence the rotated MS-STSK codeword can be expressed as

$$\mathbf{X} = \left( \tilde{A}_q s_l \right) e^{j\theta_{n_{AC}}} \quad (4)$$

$$\begin{aligned} &= \tilde{A}_{q,n_{AC}} s_l \\ &= [\mathbf{x}_1 \dots \mathbf{x}_{n_t} \dots \mathbf{x}_{N_t}]^T \\ &= [\mathbf{X}_1 \dots \mathbf{X}_{T_1} \dots \mathbf{X}_T], \end{aligned} \quad (5)$$

where  $\tilde{A}_q \in \mathbb{C}^{N_{RF}^t \times T}$  denotes the MS-STSK dispersion matrix representing the equivalent mapped version of  $A_q$ ,  $\tilde{A}_{q,n_{AC}} \in \mathbb{C}^{N_{RF}^t \times T}$  represents the MS-STSK dispersion matrix representing the  $q$ -th STSK dispersion matrix and the  $n_{AC}$ -th AC,  $\mathbf{x}_m \in \mathbb{C}^{1 \times T}$  represents the  $n_{RF}^t$ -th row of the codeword  $\mathbf{X}$  given that  $n_{RF}^t = 1, \dots, N_{RF}^t$ , where finally,  $\mathbf{X}_{T_i} = [X_{T_i,1} \dots X_{T_i,m} \dots X_{T_i,M}]^T \in \mathbb{C}^{M \times 1}$  is the  $T_i$ -th column representing the  $T_i$ -th time slot of the codeword  $\mathbf{X}$ . Again in order to overcome the frequency selectivity of the wideband mmWave channel, OFDM is employed based on the OFDM-aided STSK mapping technique in [32]. Prior to the MS encoding, a total of  $N_{sc}$  STSK codewords are fed into the

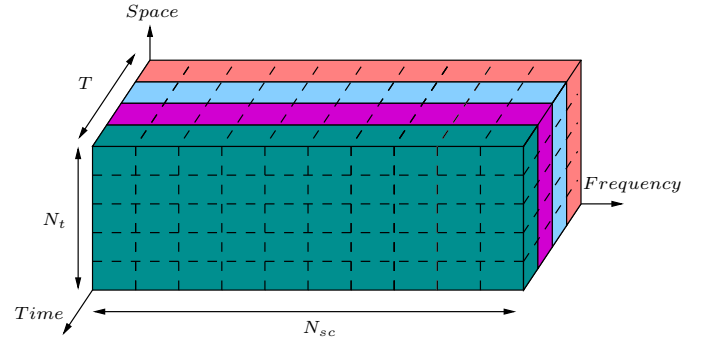


Figure 5. The transmitted OFDM symbols over the  $T$  STSK time slots.

AC	TAA Combination
0	$\{TAA_1, TAA_2\}$
1	$\{TAA_1, TAA_3\}$
2	$\{TAA_1, TAA_4\}$
3	$\{TAA_2, TAA_3\}$

Table III  
AC MAPPING TABLE OF A TRANSMITTER EQUIPPED WITH  $N_{RF}^t = 4$  AND STSK ENCODER ASSOCIATED WITH  $M = 2$ , WHERE  $TAA_i$  CORRESPONDS TO THE TAA'S INDEX.

space-time mapper of Figure 4 in order to generate  $T$  OFDM symbols carrying the  $N_{sc}$  codewords. As shown in Figure 5, the  $T_i$ -th OFDM symbol can be expressed as

$$\mathcal{F}_{T_i} = [\mathbf{X}_{T_i}(1) \dots \mathbf{X}_{T_i}(n_{sc}) \dots \mathbf{X}_{T_i}(N_{sc})] \in \mathbb{C}^{N_{RF}^t \times N_{sc}}, \quad (6)$$

where  $T_i = 1, \dots, T$  represents the STSK time slot,  $n_{sc} = 1, \dots, N_{sc}$  denotes the  $n_{sc}$ -th sub-carrier,  $N_{sc}$  denotes the total number of sub-carriers and finally,  $\mathbf{X}_{T_i}(n_{sc})$  represents the  $T_i$ -th component of  $n_{sc}$ -th MS-STSK codeword  $\mathbf{X}(n_{sc})$  defined in (1). Furthermore, the  $n_{RF}^t$ -th component of  $\mathbf{X}_{T_i}(n_{sc})$  is denoted by  $\mathbf{X}_{T_i,n_{RF}^t}(n_{sc})$ , hence  $\mathbf{X}_{T_i}(n_{sc}) = [\mathbf{X}_{T_i,1}(n_{sc}) \dots \mathbf{X}_{T_i,n_{RF}^t}(n_{sc}) \dots \mathbf{X}_{T_i,N_{RF}^t}(n_{sc})]^T$ .

The MS encoder collects  $N_{sc}$  AC indices in order to map each AC to its corresponding  $n_{sc}$  sub-carrier, based on the predefined look-up table. For example, the AC mapping scheme shown in Table III is that of a transmitter equipped with a total of  $N_{RF}^t = 4$  TAAs and an STSK encoder associated with  $M = 2$ , where the total number of ACs is equal to  $N_{AC} = 4$  ACs. In this example, if the ASU produced the AC index of 2, then  $TAA_1$  and  $TAA_4$  are activated in order to transmit the data at the  $n_{sc}$ -th sub-carrier, while when the ASU produces the AC index of 3,  $TAA_2$  and  $TAA_3$  are activated instead, as shown in Table III.

An example schematic of the mapping procedure of different ACs to several sub-carriers is shown in Figure 6, where the input bits are encoded using the MS-STSK encoder. Afterward, each STSK codeword is mapped to its corresponding TAAs. The output of the  $n_{RF}^t$ -th OFDM modulator is defined as:

$$\tilde{x}_{T_i,n_{RF}^t}[n_{sc}] = \sqrt{N_{sc}} IDFT \left\{ \mathbf{X}_{T_i,n_{RF}^t}(n_{sc}) \right\}. \quad (7)$$



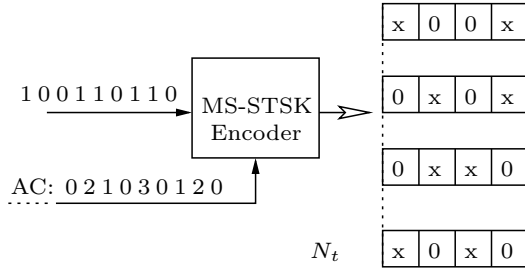


Figure 6. The MS-STSK codeword at each sub-carrier is mapped to its corresponding TAAs based on the AC  $N_{sc}$  sequence fed from the MS encoder.

Due to the short wave-lengths of mmWave signals, large numbers of AEs may be accommodated in relatively compact spaces for the sake of achieving high ABF gains, which is imperative for mitigating the high path loss of mmWaves [35]. The OFDM-MS-STSK system proposed here may be readily operated in the 28 GHz, 38 GHz, 60 GHz or 72 GHz frequency bands having wavelengths of 10.7 mm, 7.9 mm, 5 mm and 4.2 mm, respectively. Each AE in the TAA is connected to a phase-shifter and an amplifier, which steers the signal towards the receiver. For instance, at the  $n_{RF}^t$  TAA, a steering vector of  $\mathbf{w}(\theta_{n_{RF}^t}^{Tx}) = [w(\theta_{n_{RF}^t,1}^{Tx}) \dots w(\theta_{n_{RF}^t,N_{AA}^t}^{Tx})]^T \in \mathbb{C}^{N_{AA}^t \times 1}$  steers the output of the TAA, where the overall ABF precoder at the  $n_{sc}$ -th sub-carrier can be expressed as

$$\mathbf{W}(n_{sc}) = \begin{bmatrix} \mathbf{w}(\theta_1^{Tx}) & \mathbf{0} & \mathbf{0} & \dots & \mathbf{0} \\ \mathbf{0} & \ddots & \vdots & \vdots & \mathbf{0} \\ \mathbf{0} & \mathbf{0} & \mathbf{w}(\theta_{n_{RF}^t}^{Tx}) & \dots & \vdots \\ \vdots & \vdots & \vdots & \ddots & \vdots \\ \mathbf{0} & \mathbf{0} & \mathbf{0} & \mathbf{0} & \mathbf{w}(\theta_{N_{RF}^t}^{Tx}) \end{bmatrix}, \quad (8)$$

where  $\mathbf{W}(n_{sc}) \in \mathbb{C}^{N_t \times N_{RF}^t}$  and  $\mathbf{0}$  is a vector of zeros. The AEs of each TAA are spaced at a distance of  $\lambda/2$  in order to achieve a BF gain. Furthermore, the steering vectors of inactivate antennas are zeros.

### B. MS-STSK Receiver

The OFDM-MS-STSK receiver's block diagram is shown in Figure 7. The receiver is equipped with  $N_{RF}^r$  RAAs with an identical number of RF chains. Each RAA is formed of  $N_{AA}^r$  AEs employed for the sake of achieving a further receive ABF gain. The  $n_{RF}^r$ -th RAA ABF weights vector  $\mathbf{z}(\theta_{n_{RF}^r}^{Rx}) = [z(\theta_{n_{RF}^r,1}^{Rx}) \dots z(\theta_{n_{RF}^r,N_{AA}^r}^{Rx})] \in \mathbb{C}^{1 \times N_{AA}^r}$  can be generalized for all the  $N_{RF}^r$  RAAs at sub-carrier  $n_{sc}$  as

$$\mathbf{Z}(n_{sc}) = \begin{bmatrix} \mathbf{z}(\theta_1^{Rx}) & \mathbf{0} & \mathbf{0} & \dots & \mathbf{0} \\ \mathbf{0} & \ddots & \vdots & \vdots & \mathbf{0} \\ \mathbf{0} & \mathbf{0} & \mathbf{z}(\theta_{n_{RF}^r}^{Rx}) & \dots & \vdots \\ \vdots & \vdots & \vdots & \ddots & \vdots \\ \mathbf{0} & \mathbf{0} & \mathbf{0} & \mathbf{0} & \mathbf{z}(\theta_{N_{RF}^r}^{Rx}) \end{bmatrix}, \quad (9)$$

where  $\mathbf{Z}(n_{sc}) \in \mathbb{C}^{N_{RF}^r \times N_r}$  represents the ABF weights vector at the  $n_{sc}$ -th sub-carrier and  $\mathbf{0}$  is a vector of zeros.

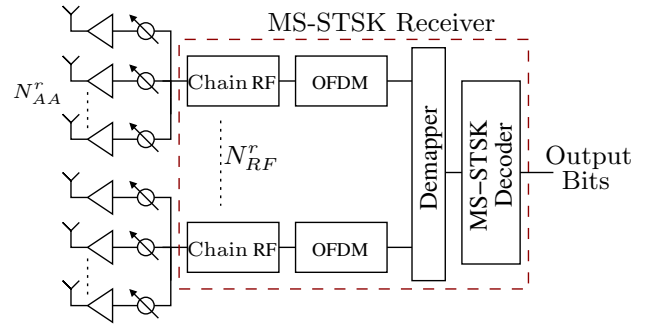


Figure 7. OFDM-MS-STSK receiver block diagram.

It was shown in [39], [40], [41], [42] that the mmWave channel can be represented by a clustered multipath channel model, where different multipath components propagate in distinct clusters segregated both in space and time, as governed by the angle-of-departure (AoD), angle-of-arrival (AoA) and the delay characteristics. The mmWave channel between the  $n_t$ -th TAE and the  $n_r$ -th receive AE is characterized by the double-directional impulse response [34], [39] as

$$h_{n_r,n_t}(t, \tau, \theta, \varphi) = \sum_{n_c=1}^{N_{cl}} \sum_{n_p=1}^{N_p(n_c)} \alpha_{n_c,n_p} \cdot \delta(\varphi - \bar{\varphi}_{n_c}^{Rx} - \varphi_{n_c,n_p}^{Rx}) \cdot \delta(\theta - \bar{\theta}_{n_c}^{Rx} - \theta_{n_c,n_p}^{Rx}) \cdot \delta(\varphi - \bar{\varphi}_{n_c}^{Tx} - \varphi_{n_c,n_p}^{Tx}) \cdot \delta(\theta - \bar{\theta}_{n_c}^{Tx} - \theta_{n_c,n_p}^{Tx}) \cdot \delta(t - \tau_{n_c} - \tau_{n_c,n_p}), \quad (10)$$

where  $\alpha_{n_c,n_p}$  is the complex gain of the  $n_p$ -th multipath component in the  $n_c$ -th cluster. Both  $(\theta_{n_c,n_p}^{Tx}, \varphi_{n_c,n_p}^{Tx})$  and  $(\theta_{n_c,n_p}^{Rx}, \varphi_{n_c,n_p}^{Rx})$  characterize the (azimuth, elevation) AoD and AoA at the transmitter and receiver, respectively, given that  $(\bar{\varphi}_{n_c}^{Tx}, \bar{\theta}_{n_c}^{Tx})$  and  $(\bar{\varphi}_{n_c}^{Rx}, \bar{\theta}_{n_c}^{Rx})$  represent their corresponding mean cluster angles. The parameter  $\tau_{n_c,n_p}$  denotes the delay of the  $n_p$ -th multipath component in the  $n_c$ -th cluster and  $\tau_{n_c}$  is the  $n_c$ -th cluster delay. Hence, the discrete-time CIR of the mmWave channel between the transmitter and receiver may be expressed as

$$\hat{H}[n_{sc}] = \sum_{n_p=0}^{\bar{N}_p-1} \hat{H}[n_p] \delta[n_{sc} - n_p], \quad (11)$$

where  $\hat{H}[n_{sc}]$  is a simplified representation of (10), which denotes all sub-paths of all clusters in  $\bar{N}_p$ , given that  $\bar{N}_p = \sum_{n_c=1}^{N_{cl}} \sum_{n_p=1}^{N_p(n_c)} 1$ . Furthermore, a single coefficient of the matrix  $\hat{H}[n_p]$  represents the channel between the  $n_t$ -th TAE and the  $n_r$ -th receive AE, and it is denoted by  $\hat{h}_{n_r,n_t}[n_p]$ . Hence, the signal received at the output of the  $n_r$ -th receive AE at the  $T_i$  STSK time slot can be expressed as

$$r_{n_r,T_i}[n_{sc}] = \sum_{n_t=1}^{N_t} \sum_{n_p=0}^{\bar{N}_p-1} \hat{h}_{n_r,n_t}[n_p] \otimes \bar{x}_{T_i,n_t}[n_{sc} - n_p] + v_{T_i}[n_{sc}], \quad (12)$$

where  $\bar{x}_{T_i,n_t}[n_{sc}]$  is the STSK symbol transmitted by the  $n_t$ -

th AE at the  $T_i$  STSK time slot,  $v_{T_i}[n_{sc}]$  is the AWGN at the  $n_{sc}$ -th sub-carrier and  $\otimes$  denotes the circular convolution operation. For ease of observation, in what follows we consider the signal produced after applying OFDM demodulation and removing the CP. Hence, the signal received at the  $n_{sc}$ -th sub-carrier within the  $T_i$ -th STSK slot can be expressed as

$$\mathbf{R}_{T_i}(n_{sc}) = \mathbf{Z}(n_{sc})\hat{\mathbf{H}}(n_{sc})\mathbf{W}(n_{sc})\mathbf{X}_{T_i}(n_{sc}) + \mathbf{V}(n_{sc}). \quad (13)$$

Assuming that the channel remains constant during the STSK time interval  $T$ , after receiving all  $T$  OFDM symbols, the demapper shown in Figure 7 applies space-time de-mapping to each STSK symbol located at the  $n_{sc}$ -th sub-carrier of all the received  $T$  OFDM symbols to a single received MS-STSK codeword and forward it to the MS-Decoder. For ease of notation, the sub-carrier index  $n_{sc}$  is dropped in what follows, hence the  $n_{sc}$ -th received MS-STSK symbol can be expressed as

$$\mathbf{R} = \mathbf{Z}\hat{\mathbf{H}}\mathbf{W}\mathbf{X} + \mathbf{V}. \quad (14)$$

The assumption made here is that the AoD and AoA knowledge is available at both the transmitter and receiver, respectively, which implies that the optimal transmit and receive steering matrices  $\mathbf{W}$  and  $\mathbf{Z}$  are obtained at both ends. Therefore, the effective channel observed after applying the transmit and receive ABF is defined as

$$\mathbf{H} = \mathbf{Z}\hat{\mathbf{H}}\mathbf{W}, \quad (15)$$

where  $\mathbf{H} \in \mathbb{C}^{N_{RF}^r \times N_{RF}^t}$ . The received signal in (14) can now be expressed as

$$\mathbf{R} = \mathbf{H}\mathbf{X} + \mathbf{V}. \quad (16)$$

Following the philosophy of [18], the received signal in (16) can be reformulated to an SM equivalent model by applying the vectorial stacking operation, where the  $n_{sc}$ -th received MS-STSK symbol can be expressed as

$$\tilde{\mathbf{R}} = \tilde{\mathbf{H}}\mathcal{X}\mathcal{I}\mathbf{K} + \tilde{\mathbf{V}}, \quad (17)$$

with

$$\tilde{\mathbf{R}} = \text{vec}(\mathbf{R}) \in \mathbb{C}^{N_{RF}^r T \times 1}, \quad (18)$$

$$\tilde{\mathbf{H}} = \mathbf{I} \otimes \mathbf{H} \in \mathbb{C}^{N_{RF}^r T \times N_{RF}^t T}, \quad (19)$$

$$\tilde{\mathbf{V}} = \text{vec}(\mathbf{V}) \in \mathbb{C}^{N_{RF}^r T \times 1}, \quad (20)$$

$$\mathcal{X} = [\text{vec}(\tilde{A}_{1,1}) \dots \text{vec}(\tilde{A}_{q,n_{AC}})] \in \mathbb{C}^{N_{RF}^r T \times N_{AC} M_Q}, \quad (21)$$

$$\dots \text{vec}(\tilde{A}_{q,N_{AC}})] \in \mathbb{C}^{N_{RF}^r T \times N_{AC} M_Q}, \quad (22)$$

given that  $\mathbf{I}$  is a  $(T \times T)$ -element identity matrix,  $\tilde{A}_{q,n_{AC}}$  is the MS-STSK dispersion matrix of the  $n_{AC}$ -th AC and  $n_{AC} = 1, \dots, N_{AC}$ .

The system in (17) is equivalent to an SM-MIMO system, where rather than activating a single antenna to transmit a single symbol as in SM, a combination of multiple antennas is activated in order to transmit a single STSK symbol, which is converted into an MS-STSK codeword after applying appropriate preprocessing. Furthermore, the matrix  $\mathcal{I} \in \mathbb{C}^{N_{AC} M_Q \times M_Q}$  is used for selecting the activated AC and it is expressed as

$$\mathcal{I} = \mathcal{I}_{n_{AC}} = [\mathbf{0} \dots \underset{\substack{\downarrow \\ n_{AC}\text{-th element}}}{\mathbf{I}_{n_{AC}}} \dots \mathbf{0}]^T, \quad (23)$$

where  $\mathbf{I}_{n_{AC}}$  is an  $(M_Q \times M_Q)$ -element identity matrix used for activating the  $n_{AC}$ -th AC. Correspondingly, the  $q$ -th dispersion matrix is activated by introducing a single modulated symbol  $s_l$  in the  $q$ -th position of  $\mathbf{K}$ , where  $\mathbf{K} \in \mathbb{C}^{M_Q \times 1}$  and it is defined as

$$\mathbf{K} = [\underbrace{0, \dots, 0}_{q-1}, s_l, \underbrace{0, \dots, 0}_{M_Q-q}]^T. \quad (24)$$

Hence, (17) can be reformulated as

$$\tilde{\mathbf{Y}} = \begin{bmatrix} \mathbf{H} & \dots & \mathbf{0} \\ \vdots & \ddots & \vdots \\ \mathbf{0} & \dots & \mathbf{H} \end{bmatrix} \cdot \begin{bmatrix} \dots & [\hat{\mathbf{A}}_{1,n_{AC}} & \dots & \hat{\mathbf{A}}_{Q,n_{AC}}] & \dots \end{bmatrix} \cdot \begin{bmatrix} \mathbf{0} \\ \vdots \\ \mathbf{I}_{n_{AC}} \\ \vdots \\ \mathbf{0} \end{bmatrix} \cdot \begin{bmatrix} 0 \\ \vdots \\ s_l \\ \vdots \\ 0 \end{bmatrix} + \tilde{\mathbf{V}}, \quad (25)$$

where  $\hat{\mathbf{A}}_{q,n_{AC}} = \text{vec}(\tilde{A}_{q,n_{AC}}) \in \mathbb{C}^{N_{RF}^r T \times 1}$ .

The MS-STSK dispersion matrix  $\tilde{A}_{q,n_{AC}} \in \mathbb{C}^{N_{RF}^r \times T}$  is the modified version of the simplified STSK dispersion matrix  $A_q$  of [18]. It can be defined as the counterpart of the dispersion matrix  $A_q$  with zeros values representing the inactive antennas, yielding

$$\tilde{A}_{q,n_{AC}} = \begin{bmatrix} \mathbf{0} \\ \vdots \\ A_{q,m} \\ \vdots \\ \mathbf{0} \end{bmatrix} \cdot e^{j(\theta_{n_{AC}})}, \quad (26)$$

where  $A_{q,m} \in \mathbb{C}^{1 \times T}$  is the  $m$ -th row of  $A_q$  and  $m = 1, \dots, M$ .

With the aid of an ML detector, the receiver becomes capable of obtaining  $\hat{q}$ ,  $\hat{l}$  and  $\hat{n}_{AC}$ , namely the estimates of the dispersion matrix index  $q$ , the modulated symbol index  $l$  and the AC index  $n_{AC}$ , respectively, as

$$\langle \hat{q}, \hat{l}, \hat{n}_{AC} \rangle = \arg \min_{q,l,n_{AC}} \|\tilde{\mathbf{R}} - \tilde{\mathbf{H}}\mathcal{X}\mathcal{I}_{n_{AC}}\mathbf{K}_{q,l}\|^2 \quad (27)$$

However, owing to the fact that hard-decision decoding is employed at the receiver, the detection complexity order can be further reduced from  $\mathcal{O}(M_Q M_c N_{AC})$  to  $\mathcal{O}(M_Q N_{AC})$ , while retaining the optimality of detection with the aid of the Hard-Limiter ML (HL-ML) detection employed in [18], yielding

$$\langle \hat{q}, \hat{n}_{AC} \rangle = \arg \min_{q,n_{AC}} (|\hat{\mathbf{r}}_{n_{AC},q} - \hat{s}_l|^2 - |\hat{\mathbf{r}}_{n_{AC},q}|^2) \|\mathbf{h}_{n_{AC},q}\|^2, \quad (28)$$



where  $\mathbf{H}_{n_{AC}} = [\mathbf{h}_{n_{AC},1} \dots \mathbf{h}_{n_{AC},M_Q}] \in \mathbb{C}^{N_r T \times M_Q}$ ,  $\hat{s}_l$  is the estimated  $M_c$ -QAM/PSK symbol and  $\hat{\mathbf{r}}_{n_{AC},q}$  is the equalized received symbol denoted by

$$\hat{\mathbf{r}}_{n_{AC},q} = \frac{\mathbf{h}_{n_{AC},q}^H \bar{\mathbf{R}}}{\|\mathbf{h}_{n_{AC},q}\|^2}. \quad (29)$$

### C. MS-STSK Phase Rotation

The phase rotation  $\theta_{n_{AC}}$  in (4) is applied to each STSK codeword transmitted over the  $n_{AC}$ -th AC in order to overcome the correlation between the specific STSK codewords sharing some TAAs [18]. Again, this correlation is introduced by transmitting different STSK codewords over the same AC and it was shown in [18] that this correlation can lead to a performance degradation. For the sake of obtaining the best rotation phase for each  $M_c$ -QAM/PSK modulation, we applied brute-force ML detection for several OFDM-MS-STSK systems associated with different modulation schemes. All simulations were carried out at high SNR with an incremental step of  $1^\circ$  for each iteration of  $\Delta\theta$  from  $0^\circ$  to  $360^\circ$ , where  $\Delta\theta = \theta_{n_{AC}+1} - \theta_{n_{AC}}$  is the phase difference between two AC rotations. Furthermore, each simulation was carried out by generating 25,000 bits over 50 iterations.

Four distinct scenarios were considered for determining the best values of  $\Delta\theta$  as follows. OFDM-MS-STSK system with  $N_{RF}^t = 4$  and STSK(2,2,2,4,BPSK) encoder,  $N_{RF}^t = 5$  and STSK(2,2,2,4,8PSK) encoder,  $N_{RF}^t = 4$  and STSK(2,2,2,4,4QAM) encoder and  $N_{RF}^t = 4$  and STSK(2,2,2,4,16QAM) encoder. The number of TAAs was set to  $N_{RF}^t = 4$ , the number of RAAs to  $N_{RF}^r = 2$ , the number of STSK spaces to  $M = 2$  and  $T = 2$  time slots were used for all systems the considered in order to exclusively evaluate the impact of the modulation scheme employed on the choice of the phase-shift  $\theta_{n_{AC}}$ . The BER performance versus the phase-shift angle of the OFDM-MS-STSK(4, 2, 2, 2, 4,4QAM) system associated with the SAC configuration and transmitting over the mmWave channel at SNR= 19 dB<sup>2</sup> is shown in Figure 8. This figure shows that the phase-shift has an impact on the performance of the system, where for instance Figure 8 shows that the minimum BER of 1.6e-05 was achieved at  $\Delta\theta = 288^\circ$  for the OFDM-MS-STSK(4, 2, 2, 2, 4, 4QAM) system at SNR= 19 dB, while the maximum BER of 5.92e-05 was achieved at  $\Delta\theta = 311^\circ$  at the same SNR. Similarly, the best phase-shift values<sup>3</sup> for the OFDM-MS-STSK(4, 2, 2, 2, 4,BPSK), OFDM-MS-STSK(4, 2, 2, 2, 4,4QAM), OFDM-MS-STSK(4, 2, 2, 2, 4,8PSK) and OFDM-MS-STSK(4, 2, 2, 2, 4,16QAM) systems were obtained from Monte Carlo simulations, where a summary of their values is provided in Table IV. Furthermore, the third row of Table IV shows the best phase-shift values for the OFDM-MS-STSK(4, 2, 2, 2, 4, 8PSK) system at SNR= 21 dB, where zero errors were detected over 50 iterations at  $\Delta\theta = 85^\circ, 111^\circ, 129^\circ, 305^\circ$  and  $349^\circ$ . The attainable throughput of the OFDM-MS-STSK system is evaluated in the following subsection.

<sup>2</sup>The SNR value is chosen such that the considered system achieves a BER of  $\leq 10^{-4}$ .

<sup>3</sup>Best phase-shift corresponds to the phase-shift resulting in the lowest BER.

$M_c$	Modulation	$\Delta\theta(\text{degree})$
2	PSK	$42^\circ/86^\circ/12^\circ/100^\circ$
8	PSK	$85^\circ, 111^\circ, 129^\circ, 305^\circ, 349^\circ$
4	QAM	$288^\circ$
16	QAM	$35^\circ, 124^\circ$

Table IV  
THE PHASE ROTATION DIFFERENCE APPLIED TO DIFFERENT ACS WITH BPSK, 8PSK, 4QAM AND 16QAM MODULATION TECHNIQUES.

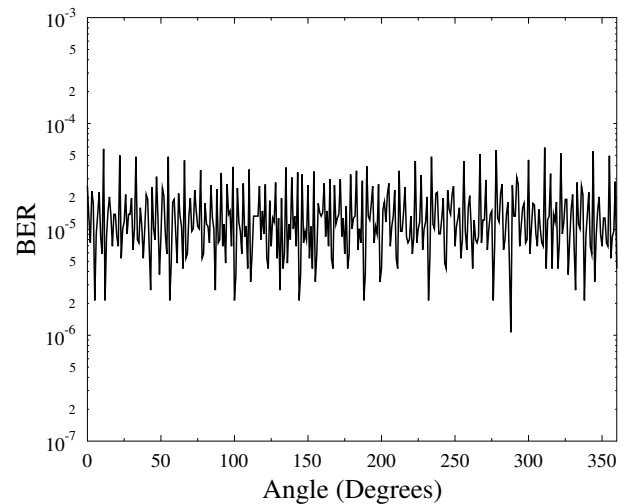


Figure 8. The BER versus phase-shift performance of OFDM-MS-STSK(4, 2, 2, 2, 4,4QAM) at SNR=19 dB with an incremental step of  $1^\circ$  for each iteration of  $\Delta\theta$  from  $0^\circ$  to  $360^\circ$ .

### D. OFDM-MS-STSK Throughput

In the OFDM-MS-STSK scheme, an OFDM symbol associated with  $N_{sc}$  MS-STSK codewords carries  $(N_{sc} + N_{cp})$  symbols, where  $N_{cp}$  is the length of the CP. Consequently, the overall throughput of the system is affected by the length of CP. Given that each sub-carrier carries  $\log_2(M_q M_c)$  bits over the interval  $T$  by the STSK codeword and  $\log_2(N_{AC})$  bits by the AC index, the system's throughput is defined as

$$R_{MS-STSK} = \frac{\log_2(M_q M_c N_{AC})}{\left(1 + \frac{N_{cp}}{N_{sc}}\right)} \text{ (bps)}, \quad (30)$$

$$= \underbrace{\frac{\log_2(M_q M_c)}{\left(1 + \frac{N_{cp}}{N_{sc}}\right)}}_{R_{STSK}} + \underbrace{\frac{\log_2(N_{AC})}{\left(1 + \frac{N_{cp}}{N_{sc}}\right)}}_{R_{AC}}, \quad (31)$$

where  $R_{MS-STSK}$  represents the throughput of the entire MS-STSK OFDM symbol in bits per symbol,  $R_{STSK}$  is the throughput of the STSK part of the OFDM-MS-STSK,  $R_{AC}$  is the rate of extra bits conveyed by the AC index and bps short for bits per symbol.

At mmWaves, the delay-spread is of an order of nanoseconds [43], [44]. In principle, channels associated with short delay spreads are preferable over large delay spread channels, since

they impose zero ISI due to their non-dispersive nature. However, owing to their huge bandwidths, operating at mmWave frequency bands requires high sampling rates, where for instance a minimum of 1 GHz sampling rate is required for using a chunk of 500 MHz bandwidth at the 28 GHz frequency band. Thereby, even a few nanoseconds of multipath delay spread becomes non-negligible at say one nanosecond sampling time. Hence, a long CP is necessary for overcoming the effect of the time dispersive wideband mmWave channel. Nevertheless, the large bandwidths of mmWave channels allow a huge number of sub-carriers compared to the sub-3 GHz frequency bands, which reduces the denominator of (30) to  $\left(1 + \frac{N_{cp}}{N_{sc}}\right) \approx 1$ . Hence, finally we arrive at

$$[R_{MS-STSK}]_{\frac{N_{cp}}{N_{sc}} \approx 0} \rightarrow \log_2(M_q M_c N_{AC}) \text{ (bps)}. \quad (32)$$

The OFDM-MS-STSK throughput per OFDM symbol associated with a CP length of  $N_{cp} = 100$  versus the number of sub-carriers  $N_{sc}$  compared to the MS-STSK scheme's throughput [18] is illustrated in Figure 9. The figure shows that as the number of sub-carriers exceeds 1024 sub-carriers, i.e.  $N_{sc} \geq 1024$ , the OFDM-aided scheme attains 90% of the maximum achievable MS-STSK throughput, which we refer to as the normalized throughput  $\partial_{MS}$  is defined by the ratio of the attainable throughput of the MS-STSK OFDM-aided scheme over that of the classical MS-STSK scheme's throughput in [18], which can be expressed as

$$\partial_{MS} = \frac{R_{MS-STSK}}{[R_{MS-STSK}]_{\frac{N_{cp}}{N_{sc}} \approx 0}} \quad (33)$$

$$= \frac{\left(\frac{\log_2(Q \cdot \mathcal{L} \cdot N_{AC})}{\left(1 + \frac{N_{cp}}{N_{sc}}\right)}\right)}{\log_2(Q \cdot \mathcal{L} \cdot N_{AC})} \quad (34)$$

$$= \frac{1}{\left(1 + \frac{N_{cp}}{N_{sc}}\right)} \quad (35)$$

$$= \frac{N_{sc}}{(N_{sc} + N_{cp})}. \quad (36)$$

Furthermore, dividing the bandwidth into 8192 sub-carriers allows the OFDM-MS-STSK scheme to achieve a throughput efficiency of nearly 98%.

The number of extra bits carried by the AC index  $R_{AC}$  versus the number of TAAs  $N_{RF}^t$  as a function of  $M$  associated with  $N_{sc} = 8192$  sub-carriers and  $N_{cp} = 100$  is shown in Figure 10. The number of TAAs spans between  $M \leq N_{RF}^t \leq 64$ , where  $M=2, 4, 6, 8, 10, \dots, 32$ . Based on (2), as the number of TAAs increases with respect to the value of  $M$  of the STSK encoder, the number of ACs increases, which means that more bits are conveyed over the activated AC index. However, having more ACs widens the search space of the detector, hence increasing its complexity order. Furthermore, as shown in Figure 10, the OFDM-aided STSK schemes proposed in [45], [46], [47], [32] constitute special cases of the OFDM-aided MS-STSK, namely when  $N_{RF}^t = M$ .

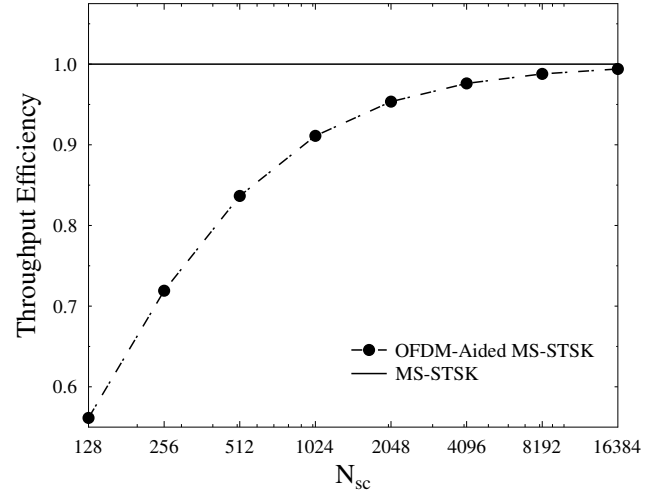


Figure 9. The efficiency of the OFDM-MS-STSK with  $N_{cp} = 100$  throughput compared to the conventional STSK throughput versus the number of sub-carriers  $N_{sc}$ .

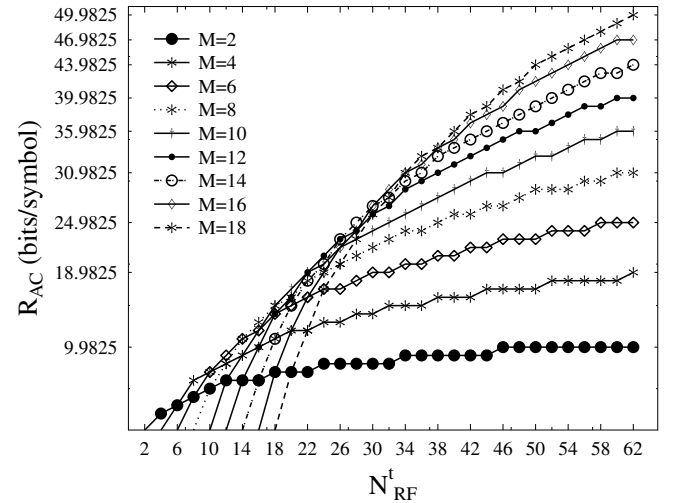


Figure 10. The achievable number of bits characterizing the AC indexes,  $R_{AC}$ , per sub-carrier associated with  $N_{sc} = 8192$  sub-carriers and  $N_{cp} = 100$ .

### E. Performance Results

In this section, we characterize the performance of our OFDM-MS-STSK system for transmission over the 28 GHz wideband channel using the Monte-Carlo technique. The simulation parameters are summarized in Table V based on the channel measurements in [34], [39].

The BER performance of the OFDM-MS-STSK system transmitting over the mmWave channel having different number of sub-carriers is shown in Figure 11 for an MS-STSK transmitter

Table V

MAIN SIMULATION PARAMETERS FOR THE OFDM-MS-STSK OVER THE 28 GHz MMWAVE CHANNEL. RMS DS\*: ROOT MEAN SQUARE DELAY SPREAD. AoA & AoD AS\*\*= AoA & AoD ANGULAR SPREAD

Parameters	Values
Carrier Frequency	28 GHz
Bandwidth	500 MHz
$P_t$	30 dB
$G_{Rx}$	24 dBi
$G_{Tx}$	24 dBi
Transmitter	MS-STSK
$N_{sc}$	8192
$N_{cp}$	100
Distance	<200 m
$N_{cl}$	Poiss( $\mu = 3.4, \sigma = 2.1$ )
$N_p(n_c)$	Exp( $\mu = 66.3, \sigma = 68.0$ )
RMS DS*	Exp( $\mu = 13.4, \sigma = 11.5$ )
AoA & AoD AS**	Exp( $\mu = 34.6, \sigma = 27.8$ )
$\bar{\varphi}^{Rx}$ and $\bar{\varphi}^{Tx}$	U(0, 360)

associated with  $N_{RF}^t = 4$  single AE TAAs equipped with an STSK(2,2,2,4,QAM) encoder. Furthermore, based on the values presented in Table IV, the phase rotation difference between each of the  $N_{AC} = 4$  ACs is  $\Delta\theta = 288^\circ$ . Moreover, the receiver employed applies ML detection to each received MS-STSK codeword at each sub-carrier.

When a single-carrier system is used, the performance of the conventional MS-STSK [18] communicating over the mmWave channel has an error floor, as shown by the curve with the (\*) marker in Figure 11. Furthermore, observe that the number of sub-carriers is the huge 500 MHz bandwidth affects the performance of the system. Explicitly, subdividing it into a small number of sub-carriers produces an error floor at  $N_{sc} = 32$  and  $N_{sc} = 64$  due to the wideband nature of the sub-bands. On the other hand, using  $N_{sc} = 128$  sub-carriers is sufficient in the 28 GHz band for a bandwidth of 500 MHz. Furthermore, the performance of the system remains unaffected by dispersion at  $N_{sc} = 8192$  sub-carriers, which facilitates more efficient transmission at a given CP length owing to the reduced overhead.

The simulation results recorded for our proposed OFDM-MS-STSK system in conjunction with different system configurations compared to the corresponding OFDM-STSK at same throughput is shown in Figure 12. The HL-ML detector of Section II-B is employed, which matches the optimal ML performance of [18]. Figure 12 shows the BER performance of an OFDM-MS-STSK system equipped with  $N_{RF}^t = 4$ ,  $N_{RF}^t = 5$  and  $N_{RF}^t = 7$  TAAs, each with a single AE and STSK(2,2,2,4,QAM) encoder achieving a throughput of 6, 7 and 8 bps, respectively. The system associated with these configurations is compared to an equivalent OFDM-STSK system relying on STSK(2,2,2,4,16QAM), STSK(2,2,2,16,8PSK) and STSK(2,2,2,16,16QAM) encoders, respectively, for transmission over the mmWave channel [19] in conjunction with  $N_{sc} = 8192$  sub-carriers. Furthermore, based on Table IV, the

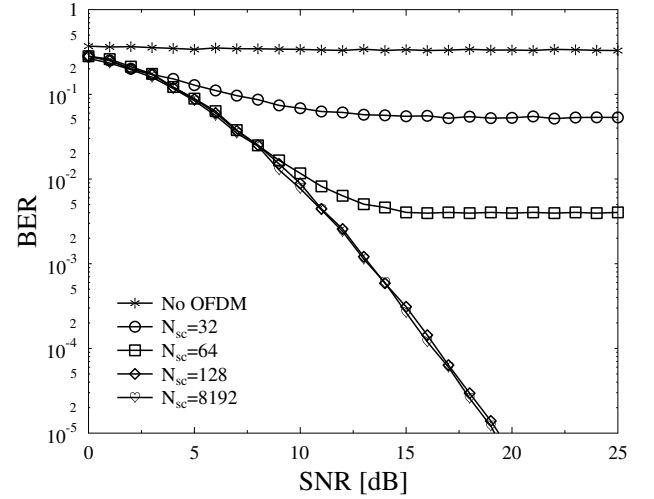


Figure 11. The BER performance of an OFDM-MS-STSK with  $N_{RF}^t = 4$  TAAs with single AE, STSK(2, 2, 2, 4, 4) encoder and  $\Delta\theta = 7^\circ$ .

phase rotation differences used for 8PSK, 4QAM and 16QAM are  $\Delta\theta_{AC} = 85^\circ, 288^\circ$  and  $35^\circ$ , respectively. The proposed OFDM-MS-STSK system outperforms the conventional STSK scheme by nearly 5 dB, 10 dB and 13 dB at a throughput of 6, 7 and 8 bits, respectively.

When employing the optimal ML detector at all receivers, the complexity order of all OFDM-MS-STSK detectors used in all cases is equivalent to the corresponding OFDM-STSK detectors' complexity order. For example, the complexity order of the OFDM-MS-STSK system having  $N_{RF}^t = 7$  TAAs and STSK(2,2,2,4,4) is  $\mathcal{O}(N_{AC} \times M_Q \times M_c) = \mathcal{O}(8 \times 4 \times 4)$ , which is equal to its equivalent throughput OFDM-STSK(2,2,2,16,8) system of  $\mathcal{O}(M_Q \times M_c) = \mathcal{O}(8 \times 16)$ . Furthermore, the complexity order of the OFDM-MS-STSK system having  $N_{RF}^t = 4$  and STSK(2,2,2,4,4) is  $\mathcal{O}(4 \times 4 \times 4)$ , which is equal to its equivalent throughput OFDM-STSK(2,2,2,4,16) system of  $\mathcal{O}(4 \times 16)$ .

Similarly, when employing the HL-ML detector, which was used in the simulations, the complexity order of both the OFDM-MS-STSK detector, as well as of the equivalent OFDM-STSK detector is reduced by  $M_c$ . For example, the complexity order of the OFDM-MS-STSK system associated with  $N_{RF}^t = 7$  and STSK(2,2,2,4,4) is  $\mathcal{O}(N_{AC} \times M_Q) = \mathcal{O}(8 \times 4)$ , while the equivalent-throughput system OFDM-STSK(2,2,2,16,8) has a complexity order of  $\mathcal{O}(M_Q) = \mathcal{O}(16)$ , which is lower than that of the former. This reduced complexity order is achieved as a result of the system configuration choice, not as a benefit of the MS-STSK technique itself, where changing the MS-STSK encoder's settings is capable of further reducing the complexity order at a given throughput.

By employing multiple AEs at each TAA and RAA, the system is capable of acquiring extra SNR gain with the aid of analogue beamforming. The effect of adding extra AEs

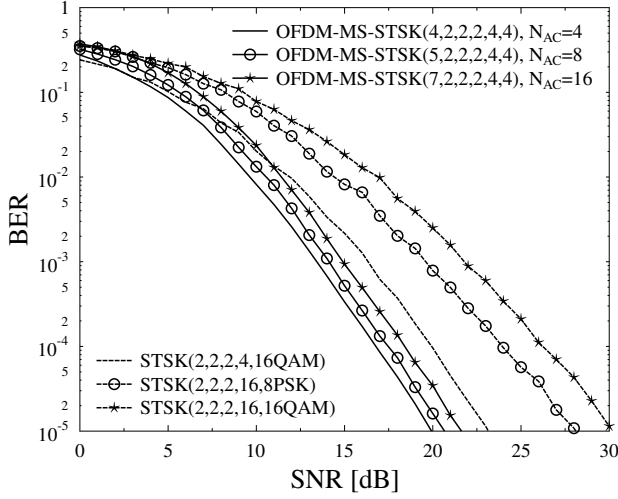


Figure 12. The BER performance of the OFDM-MS-STSK system equipped with  $N_{RF}^t = 4$ ,  $N_{RF}^t = 5$  and  $N_{RF}^t = 7$  TAAs each with a single AE and STSK(2,2,2,4QAM) encoder achieving a throughput of 6, 7 and 8 bps, respectively, compared to their OFDM-STSK equivalent systems with STSK(2,2,2,4,16QAM), STSK(2,2,2,16,8PSK) and STSK(2,2,2,16,16QAM) encoders, respectively, over mmWave channel. Based on Table IV, the phase rotation differences used for 8PSK, 4QAM and 16QAM are  $\Delta\theta_{AC} = 85^\circ$ ,  $288^\circ$  and  $35^\circ$ .

to each AA by invoking optimal analogue beamforming is shown in Figure 13, which portrays the BER performance of an OFDM-MS-STSK system associated with an  $N_{RF}^t = 7$  and STSK(2,2,2,4QAM) encoder equipped by different numbers  $N_{AA}^t$  and  $N_{AA}^r$  of AEs.

Given that the optimal analogue beamforming gain is equal to  $+10 \log(N_{AA}^t N_{AA}^r)$ , it is shown in Figure 13 that employing  $(N_{AA}^t = 2, N_{AA}^r = 1)$ ,  $(N_{AA}^t = 2, N_{AA}^r = 2)$ ,  $(N_{AA}^t = 4, N_{AA}^r = 2)$  and  $(N_{AA}^t = 10, N_{AA}^r = 2)$  lends about 3 dB, 6 dB, 9 dB and 13 dB SNR gain to the system, which are of great importance at mmWaves in order to overcome the high path loss.

### III. MULTI-SPACE-FREQUENCY STSK OVER MMWAVES

In this section, we introduce our novel Multi-Space-Frequency STSK (MSF-STSK) system. As described in Section II, the wideband mmWave channel may be partitioned into sub-bands in order to employ OFDM in the proposed OFDM-MS-STSK system. Additionally, as in Section II, the number of ACs used can be lower than the total number of ACs, where  $N_{AC}$  is limited to integer powers of 2, so that  $2^k$  binary sets can be generated. Hence, the extra number of ACs may be utilized in order to convey extra information over the sub-carrier index domain in a similar way to the technique used in the Generalized Space-Frequency Index Modulation (GSFIM) [30].

In GSFIM, the bits are encoded over both the TAE index and the sub-carrier index for the sake of enhancing the achievable throughput [30]. In our MSF-STSK system, information is

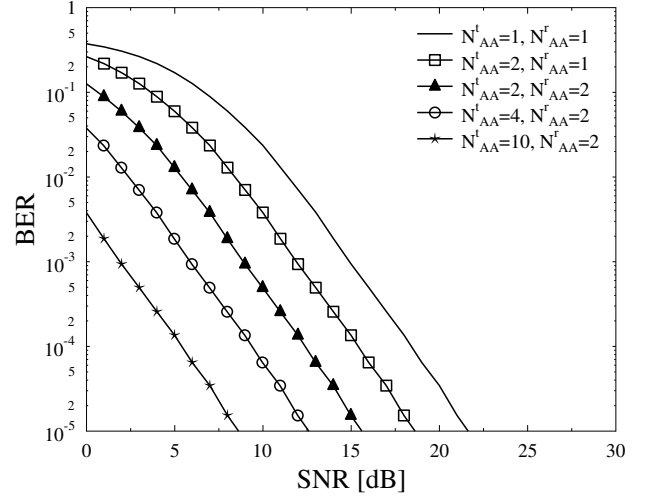


Figure 13. The BER performance of the OFDM-MS-STSK(7, 2, 2, 2, 4, 4QAM) system equipped with TAAs and RAAs having multiple sizes.

transmitted over the following three components: The first two parts are the STSK codeword and the AC index, similar to the MS-STSK scheme, while the third component is the Frequency Index (FI) of the sub-carriers with a block of sub-carriers where the extra ACs are detected, as described next.

#### A. MSF-STSK Transmitter

The proposed MSF-STSK transmitter's block diagram is identical to that of the OFDM-MS-STSK scheme shown in Figure 4. However, the MS-digital encoder is replaced by an MSF-digital encoder, which only differ at the digital encoding level. Hence, the OFDM-MS-STSK and MSF-STSK schemes are digitally interchangeable.

Given that the MSF-STSK transmitter is equipped with  $N_{RF}^t$  TAAs, the MSF-STSK encoder is fed with a block of  $B_{MSF-STSK}$  bits, which divides the input bits into  $B_{STSK}^4$ ,  $B_{ASU}^5$  and  $B_{FI}^6$  bits with the aid of the serial-to-parallel (S/P) converter in order to encode the STSK codeword as well as to select the MS-STSK sub-carrier AC and the FI of the sub-carriers block<sup>7</sup>, respectively. The  $N_{sc}$  sub-carriers are partitioned into blocks of sub-carriers each containing  $N_B = 2^{\bar{q}}$  sub-carriers, where we have

$$B_{FI} = \lfloor \log_2(N_{FI} N_B) \rfloor, \quad (37)$$

and  $N_{FI} = 2^{\bar{p}}$  is the number of ACs dedicated to FI encoding with  $n_B = 1, \dots, N_B$ . For ease of implementation, consider an MSF-STSK system with  $N_{RF}^t = 4$  TAAs,  $M = 2$  STSK spaces and a block size of  $N_B = 4$ . Here, the total number of ACs is 6, of which the MS-STSK scheme utilizes only  $N_{AC} =$

<sup>4</sup>  $B_{STSK}$  bits are used to select one out of  $Q$  STSK codewords.

<sup>5</sup>  $B_{ASU}$  bits are used to activate one out of  $N_{AC}$  antenna combinations.

<sup>6</sup>  $B_{FI}$  bits are used to select the frequency index of the sub-carriers block of size  $N_B$ .

<sup>7</sup> A block of sub-carriers is described as a set of consecutive  $N_B$  sub-carriers, which are used to encode the frequency index.

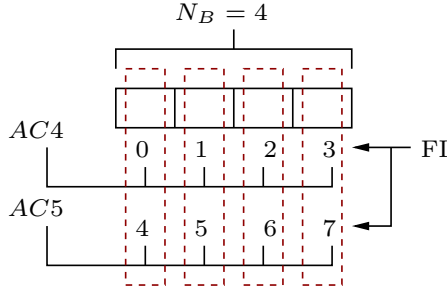


Figure 14. The 4-th AC describes the first four FI realizations FI= 0, 1, 2 or 3 when located at  $n_B = 1, 2, 3$  or 4, while the 5-th AC describes the next four FI realizations FI= 4, 5, 6 or 7 when located at  $n_B = 1, 2, 3$  or 4.

AC	TAA Combination
0	$\{TAA_1, TAA_2\}$
1	$\{TAA_1, TAA_3\}$
2	$\{TAA_1, TAA_4\}$
3	$\{TAA_2, TAA_3\}$
4	$\{TAA_2, TAA_4\}$
5	$\{TAA_3, TAA_4\}$

Table VI

MSF MAPPING TABLE OF A TRANSMITTER EQUIPPED WITH  $M = 2$  AND  $N_{RF}^t = 4$ , WHERE AC = 0, 1, 2 AND 3 ARE DEDICATED FOR THE MS-STSK PART AND AC= 4 AND 5 ARE DEDICATED FOR FREQUENCY INDEXING.

4. Hence, in MSF-STSK, the extra  $N_{FI} = 2$  ACs may be used for encoding the FI, which leads to  $B_{FI} = \lfloor \log_2(2 \times 4) \rfloor = 3$  and  $2^3 = 8$  FI realizations. As shown in Table VI, the first four combinations 0, 1, 2 and 3 are used for mapping a symbol to a specific sub-carrier based on the MS-STSK scheme, while the remaining two ACs, namely 4 and 5 are used for applying the block frequency indexing, or the FI encoding. As shown in Figure 14, the 4-th AC, describes the first four FI realizations of FI= 0, 1, 2 or 3 when located at  $n_B = 1, 2, 3$  or 4, while the 5-th AC describes the next four FI realizations FI= 4, 5, 6 or 7 when located at  $n_B = 1, 2, 3$  or 4. In other words, the location of each of the  $N_{FI}$  ACs, given by the 4-th and 5-th AC in this example, in a block of  $N_B$  sub-carriers, given by  $N_B = 4$  sub-carriers, defines the frequency index of the each sub-carrier block.

For further illustration, let us consider three frequency blocks of size  $N_B = 4$  sub-carriers encoded using the MSF-encoder. Assuming that three input bit streams of  $L1$ ,  $L2$  and  $L3$  are defined as

$$L1 = \underbrace{\{110\}}_{FI} - \underbrace{00\ 0\cdots 00}_{MS\ STSK} - \underbrace{01\ 0\cdots 00}_{MS\ STSK} - \underbrace{0\cdots 00}_{STSK} - \underbrace{11\ 0\cdots 00}_{MS\ STSK}, \quad (38)$$

$$L2 = \underbrace{\{000\}}_{FI} - \underbrace{0\cdots 00}_{STSK} - \underbrace{00\ 0\cdots 00}_{MS\ STSK} - \underbrace{11\ 0\cdots 00}_{MS\ STSK} - \underbrace{10\ 0\cdots 00}_{MS\ STSK}, \quad (39)$$

$$L3 = \underbrace{\{011\}}_{FI} - \underbrace{10\ 0\cdots 00}_{MS\ STSK} - \underbrace{11\ 0\cdots 00}_{MS\ STSK} - \underbrace{01\ 0\cdots 00}_{MS\ STSK} - \underbrace{0\cdots 00}_{STSK}, \quad (40)$$

where the notation  $\underbrace{0\cdots 00}_{STSK}$  is used for describing a random bit sequence employed for generating the STSK codeword.

By referring to Figure 15,  $L1$  is encoded into the first  $N_B$  sub-carriers block as follows. The first 3 bits describe the FI encoding, where 110 refers to the 6-th FI realisation, which can be encoded using the 5-th AC at  $n_B = 3$ . The other 3 sub-carriers are encoded based on the conventional MS-STSK scheme, where ACs 0, 1 and 3 are mapped to  $n_B = 1, n_B = 2$  and  $n_B = 4$ , respectively. Furthermore,  $L2$  is encoded into the next  $N_B$  sub-carrier block as follows. The first 000 bits refer to the 1-st FI realization, which can be encoded using the 4-th AC at  $n_B = 1$ . The other 3 sub-carriers at  $n_B = 2, n_B = 3$  and  $n_B = 4$  are mapped to ACs 0, 3 and 2, respectively. Lastly,  $L3$  is encoded into the third  $N_B$  sub-carrier block as follows. The first 011 bits refer to the 3-rd FI realization, which can be encoded using the 4-th AC at  $n_B = 4$ , while ACs 2, 3 and 1 are mapped to  $n_B = 1, n_B = 2$  and  $n_B = 3$ , respectively. Note that in other TAA-to-M configurations, where the number of extra ACs exceeds the required  $N_{FI}$  for FI encoding, it is recommended to choose  $N_{FI}$  out of the available extra ACs. For example, consider an MSF-STSK system equipped with  $N_{RF}^t = 6$  RF chains and associated with an STSK encoder having  $M = 2$ . The total number of ACs is equal to 15, which means that  $N_{AC} = 8$  ACs are used for MS-STSK

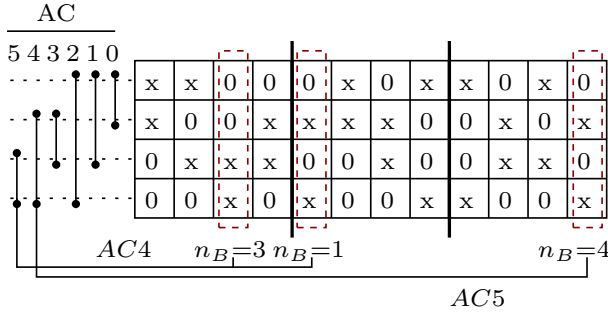


Figure 15. MSF-STSK encoding of  $L1$ ,  $L2$  and  $L3$  in (38), (39) and (40), respectively.

encoding, while  $N_{FI} = 2$  or 4 ACs out of the extra 7 ACs may be assigned for FI encoding. The procedure of constructing the OFDM symbol and the switching process in the MSF-STSK encoding is identical to the OFDM-MS-STSK scheme presented in Section II-A. In the next subsection, we introduce the MSF-STSK receiver.

### B. MSF-STSK Receiver

Similarly, the receiver block diagram of the MSF-STSK system is equivalent to that of the OFDM-MS-STSK receiver shown in Figure 7, where the MS-STSK digital decoder is replaced by an MSF-STSK decoder. Assuming the same receiver configurations as in Section II-B, the detection procedure of the MSF-STSK decoder is applied on a per sub-carrier block basis.

Consider that the  $N_{sc}$  sub-carriers are subdivided into  $N_{SB}$  blocks, each having  $N_B$  sub-carriers and recalling (16), the received signal after applying receive beamforming and OFDM demodulation at the  $n_B$ -th sub-carrier in the  $n_{sb}$ -th block is modeled as

$$\mathbf{R}_{n_B}^{n_{sb}} = \mathbf{H}_{n_B}^{n_{sb}} \mathbf{X}_{n_B}^{n_{sb}} + \mathbf{V}_{n_B}^{n_{sb}}, \quad (41)$$

where  $\mathbf{R}_{n_B}^{n_{sb}}$ ,  $\mathbf{H}_{n_B}^{n_{sb}}$ ,  $\mathbf{X}_{n_B}^{n_{sb}}$  and  $\mathbf{V}_{n_B}^{n_{sb}}$  are the received signal, the mmWave channel, the received symbol and the noise at the  $n_B$ -th sub-carrier in the  $n_{sb}$ -th block, with  $n_{sb} = 1, \dots, N_{SB}$ . Then, the detection of each block is carried out in two stages with the aid of an optimal ML detector. The first stage detects the block's FI by obtaining  $(\hat{n}_{FI}, \hat{n}_B)$ , which represents the estimates of the AC used  $n_{FI} = 1, \dots, N_{FI}$  and the sub-carrier index  $n_B$ , while  $\hat{q}_{FI}$  and  $\hat{l}_{FI}$  are the estimates of the dispersion matrix and of the QAM/PSK symbol indices of the  $(\hat{n}_{FI}, \hat{n}_B)$  STSK symbol, yielding

$$\langle \hat{q}_{FI}, \hat{l}_{FI}, (\hat{n}_{FI}, \hat{n}_B) \rangle = \arg \min_{n_B, q, l, n_{FI}} \left\| \bar{\mathbf{R}}_{n_B}^{n_{sb}} - \bar{\mathbf{H}} \mathcal{X}_{n_{FI}} \mathbf{K}_{q, l} \right\|^2, \quad (42)$$

where  $n_B = 1, \dots, N_B$ ,  $\bar{\mathbf{R}}_{n_B}^{n_{sb}} = \text{vec}(\mathbf{R}_{n_B}^{n_{sb}})$  and  $\mathcal{I}_{n_{FI}} = [0 \dots \mathbf{I}_{n_{FI}} \dots 0]^T \in \mathbb{C}^{N_{FI} M_Q \times M_Q}$ , where an  $(M_Q \times M_Q)$ -element identity matrix  $\mathbf{I}_{n_{FI}}$  is used to activate the  $n_{FI}$ -th AC.

After determining the FI index of the  $n_{sb}$ -th block, the second stage is activated for detecting MS-STSK symbols at the other sub-carriers as

$$\langle \hat{q}_{\bar{n}_B}, \hat{l}_{\bar{n}_B}, \hat{n}_{AC} \rangle = \arg \min_{q, l, n_{AC}} \left\| \bar{\mathbf{R}}_{\bar{n}_B}^{n_{sb}} - \bar{\mathbf{H}} \mathcal{X}_{n_{AC}} \mathbf{K}_{q, l} \right\|^2, \quad (43)$$

where  $\bar{n}_B = 1, \dots, n_{FI}-1, n_{FI}+1, \dots, N_B$  and  $\hat{q}_{\bar{n}_B}$ ,  $\hat{l}_{\bar{n}_B}$  and  $\hat{n}_{AC}$  represent the estimates of the dispersion matrix index, of the modulated symbol index and of the AC index  $n_{AC}$  at the  $\bar{n}_B$ -th sub-carrier in the  $n_{sb}$ -th block, respectively.

However, owing to the fact that each sub-carrier in the MSF-STSK symbol is equivalent to the OFDM MS-STSK symbol, the reduced-complexity HL-ML optimal detector of [18] and defined in equation (28) can be invoked for further reducing the complexity order of the MSF-STSK detector. Hence, the stage one decoding can be formulated as

$$\langle \hat{q}_{n_B}, \hat{n}_{FI} \rangle = \arg \min_{q, n_{AC}} \left( \left| \hat{\mathbf{r}}_{n_B, q} - \hat{s}_{l_{n_B}} \right|^2 - \left| \hat{\mathbf{r}}_{n_B, q} \right|^2 \right) \left\| \mathbf{h}_{n_{FI}, q} \right\|^2, \quad (44)$$

where  $\hat{s}_{l_{n_B}}$  is the  $M_c$ -QAM/PSK symbol estimated at the  $n_B$ -th sub-carrier in the  $n_{sb}$  block and  $\hat{\mathbf{r}}_{n_B, q}$  is the equalized received symbol denoted by

$$\hat{\mathbf{r}}_{n_B, q} = \frac{\mathbf{h}_{n_B, q}^H \bar{\mathbf{R}}_{n_B}^{n_{sb}}}{\left\| \mathbf{h}_{n_B, q} \right\|^2}. \quad (45)$$

By contrast, the stage two detection at the  $\bar{n}_B$  sub-carrier can be translated into

$$\langle \hat{q}_{\bar{n}_B}, \hat{n}_{AC} \rangle = \arg \min_{q, n_{AC}} \left( \left| \hat{\mathbf{r}}_{\bar{n}_B, q} - \hat{s}_{l_{\bar{n}_B}} \right|^2 - \left| \hat{\mathbf{r}}_{\bar{n}_B, q} \right|^2 \right) \left\| \mathbf{h}_{n_{AC}, q} \right\|^2, \quad (46)$$

where  $\hat{s}_{l_{\bar{n}_B}}$  is the  $M_c$ -QAM/PSK symbol estimated at the  $\bar{n}_B$ -th sub-carrier in the  $n_{sb}$  block.

### C. MSF-STSK Throughput

The main advantage of MSF-STSK over the OFDM-MS-STSK scheme is its enhanced throughput, where encoding the FI of each block of sub-carriers adds extra information to the transmitted symbol. The bit rate per sub-carrier of MSF-STSK is defined as

$$R_{n_s} = \frac{\log_2(M_q M_c)}{N_B} \{ (N_B - 1) \log_2(N_{AC}) + \log_2(N_B N_{FI}) \} \text{ (bit/sub-carrier)}, \quad (47)$$

while the bit rate per block as

$$R_{n_{bs}} = \log_2(M_q M_c) \{ (N_B - 1) \log_2(N_{AC}) + \log_2(N_B N_{FI}) \} \text{ (bit/block)}, \quad (48)$$

whereas the symbol rate of MSF-STSK, while taking into consideration the CP length is defined as

$$R_{MSF-STSK} = \frac{R_{n_{bs}}}{N_B (N_{sc} + N_{cp})} \text{ (bps)}. \quad (49)$$

For the sake of achieving a higher throughput in MSF-STSK than MS-STSK, the size of the block should be constrained by the condition of

$$\log_2(N_B N_{FI}) > \log_2(N_{AC}). \quad (50)$$

The specific choice of the block size  $N_B$  is crucial in order to achieve the optimal system throughput. At a given number

of antenna combinations for  $N_{AC}$  and  $N_B$ , the total number of bits transmitted per block using the MSF-STSK scheme reaches its maximum, when  $\Delta\tilde{R}$  reaches its maximum value, given that

$$\Delta\tilde{R} = \tilde{R}_{MSF} - \tilde{R}_{MS}, \quad (51)$$

and

$$\Delta\tilde{R}|_{\max} = \max \left\{ \tilde{R}_{MSF} - \tilde{R}_{MS} \right\}, \quad (52)$$

where  $\tilde{R}_{MSF}$  and  $\tilde{R}_{MS}$  denote the total number of bits carried by the  $N_{sc}$  sub-carriers using MSF-STSK and OFDM-MS-STSK, respectively, using both AC indexing and FI indexing without taking the STSK codeword into consideration, while  $\Delta\tilde{R}$  is the difference between both numbers. The values of  $\tilde{R}_{MSF}$  and  $\tilde{R}_{MS}$  can be expressed as

$$\tilde{R}_{MSF} = \frac{N_{sc}}{N_B} \{ (N_B - 1) \log_2(N_{AC}) + \log_2(N_B N_{FI}) \}, \quad (53)$$

and

$$\tilde{R}_{MS} = \left( \frac{N_{sc}}{N_B} \right) N_B \log_2(N_{AC}). \quad (54)$$

Hence, we have

$$\Delta\tilde{R} = \left( \frac{N_{sc}}{N_B} \right) \log_2 \left( \frac{N_{FI}}{N_{AC}} N_B \right). \quad (55)$$

In general, the numbers of ACs,  $N_{AC}$  and  $N_{FI}$ , dedicated for MS and FI encoding is limited by the number of TAAs and the size of the STSK codeword  $M$ , which means that their values are constant for a specific transmitter configuration. Therefore, we can modify the size of the block to satisfy (52) by determining the maximum value of  $\Delta\tilde{R}$  in terms of  $N_B$  as

$$\frac{\partial \Delta\tilde{R}}{\partial N_B} = 0, \quad (56)$$

where

$$\frac{\partial \Delta\tilde{R}}{\partial N_B} = \frac{N_{sc}}{N_B^2} \log_2 \left( \frac{N_{AC}}{N_{FI}} N_B \right) + \frac{N_{sc}}{N_B^2 \log_e(2)}. \quad (57)$$

Now, by combining (56) and (57) we get

$$\log_2 \left( N_B \frac{N_{FI}}{N_{AC}} \right) + \frac{1}{\log_e(2)} = 0, \quad (58)$$

$$\log_2(N_B) = \frac{1}{\log_e(2)} + \log_2 \left( \frac{N_{AC}}{N_{FI}} \right), \quad (59)$$

and finally

$$N_B \rightarrow \left( \frac{N_{AC}}{N_{FI}} \right) 2^{\frac{1}{\log_e(2)}}. \quad (60)$$

The best block size  $N_B$  of MSF-STSK for different values of  $N_{AC}/N_{FI}$  is shown in Figure 16. Given that (60) results in a decimal number, the number of sub-carriers per block scales down or up to the nearest integer power of two.

For example, consider an MSF-STSK system associated with  $N_{RF}^t = 4$  TAAs,  $M = 2$ ,  $N_{sc} = 8192$  sub-carriers. The total number of ACs is 6, where the first four ACs are dedicated to the MS-STSK component associated with  $N_{AC} = 4$  and the remaining two ACs are used for FI encoding. The number of bits conveyed by ACs and FI indices per OFDM symbol over  $N_{sc}$  sub-carriers versus  $N_B$  is shown in Figure 17. The optimal block size is either  $N_B = 4$  or 8, where an extra 2048 bits

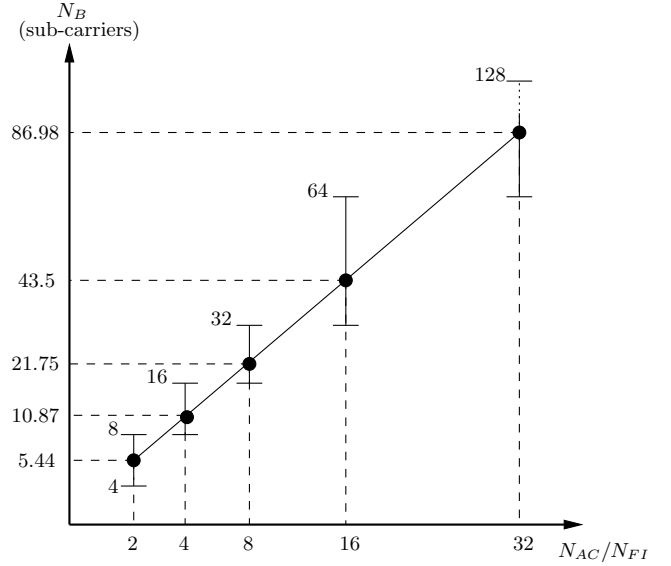


Figure 16. The optimal values of  $N_B$  versus the  $N_{AC}/N_{FI}$  ratio.

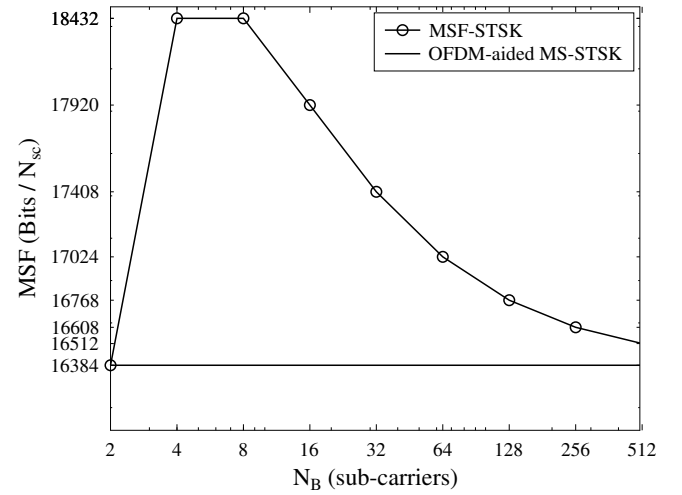


Figure 17. The number of bits conveyed by ACs and FI indices per OFDM symbol over  $N_{sc}$  sub-carriers versus  $N_B$ .

per STSK-OFDM symbol may be carried via the FI blocks. However, the optimal size of the block here is  $N_B = 4$ , since it will be shown in the following section that it has a lower complexity order at the same throughput.

#### D. MSF-STSK Complexity

The complexity order of the OFDM-MS-STSK detector for each codeword detected at each sub-carrier is  $\mathcal{O}_{MS-STSK}(M_Q M_c N_{AC})$  [18], which can be reduced to  $\mathcal{O}_{MS-STSK}(M_Q N_{AC})$  when employing the HL-ML detector shown in (28). However, in conjunction with MSF-STSK, the complexity order is increased as a result of increasing the



throughput with the aid of an extra search space, which is the FI.

Given that the MSF-STSK detector applies full search over a block of  $N_B$  sub-carriers in two consecutive stages for the sake of detecting the transmitted MSF-STSK symbols, the complexity order per block of an ML optimal detector is defined as

$$\bar{\mathcal{O}}_{MSF}^{N_B} = N_B N_{FI} M_Q M_c + \quad (61)$$

$$(N_B - 1) M_Q M_c N_{AC}, \quad (62)$$

$$= M_Q M_c \{N_B N_{FI} + N_B N_{AC} - N_{AC}\}, \quad (63)$$

which can be scaled down in the context of single codeword per sub-carrier detection to

$$\bar{\mathcal{O}}_{MSF} = M_Q M_c \left\{ N_{FI} + N_{AC} \left( 1 - \frac{1}{N_B} \right) \right\}. \quad (64)$$

Furthermore, by employing the HL-ML detector of (44) and (46) for both stages, the complexity order per block is reduced to

$$\mathcal{O}_{MSF}^{N_B} = M_Q \{N_B N_{FI} + N_B N_{AC} - N_{AC}\}, \quad (65)$$

while the complexity order per codeword/sub-carrier to

$$\mathcal{O}_{MSF} = M_Q \left\{ N_{FI} + N_{AC} \left( 1 - \frac{1}{N_B} \right) \right\}. \quad (66)$$

For a given number of sub-carriers  $N_{sc}$ , employing the MSF-STSK scheme would enhance the throughput of the OFDM-MS-STSK scheme at the cost of an increased complexity order. Using the same example as in Section III-C, choosing  $N_B = 4$  or  $N_B = 8$  would achieve the same throughput. However, the complexity order of  $\bar{\mathcal{O}}_{MSF}^{N_B=8}$  is higher than  $\bar{\mathcal{O}}_{MSF}^{N_B=4}$ . Hence, based on the configurations specified in this example, the block size of  $N_B = 4$  is preferable.

### E. Performance Results

The simulation parameters used in this section are the same as those used for the OFDM-MS-STSK system summarized in Table V. Figure 18 shows the performance of the MSF-STSK system for different configurations for transmission over the mmWave wideband channel. Given that all systems have  $N_{AC} = 4$  ACs for the MS-STSK component of MSF-STSK, the block size of each of the MSF-STSK systems considered was chosen based on Sections III-C and III-D, where MSF-STSK associated with  $N_{RF}^t = 8$  should have a block size of  $N_B = 16$  when using only  $N_{FI} = 2$  ACs for frequency indexing, the MSF-STSK arrangement associated with  $N_{RF}^t = 6$  should have a block size of  $N_B = 4$ , when  $N_{FI} = 4$  ACs are employed for frequency indexing. By contrast, the MSF-STSK associated with  $N_{RF}^t = 4$  should have a block size of  $N_B = 4$  when using only  $N_{FI} = 2$  ACs for frequency indexing. At a given number of ACs for MS and FI, these configurations were selected for achieving detection at the lowest possible complexity order.

The number of bits transmitted over the MS-STSK component of the system is equal to 32,768 spread over 8,192 sub-carriers, which are divided into 2 bits, 2 bits and 2 bits conveyed by the dispersion matrix, the modulated symbol and the AC over each sub-carrier, respectively. However, the three systems of Figure 18 have a total of  $N_{RF}^t = 4$ ,  $N_{RF}^t = 6$  and  $N_{RF}^t = 8$

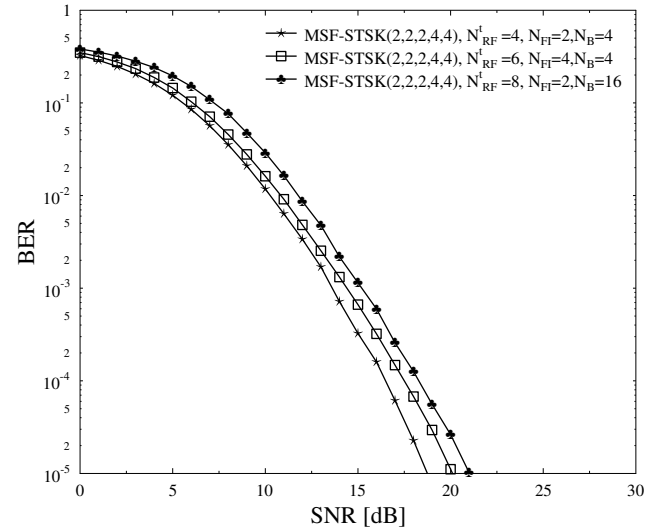


Figure 18. The BER performance of the MSF-STSK system with different transmitter configuration and HL-ML detection employed at the receiver.

transmit antennas in conjunction with  $N_{FI} = 2$ ,  $N_{FI} = 4$  and  $N_{FI} = 2$  ACs employed for frequency indexing, each with  $N_B = 4$ ,  $N_B = 4$  and  $N_B = 16$  sub-carriers per block. Hence, they can convey 6,144, 8,192 and 2,560 extra bits over the 8,192 sub-carriers using frequency indexing, respectively. Furthermore, the BER performance can be enhanced by applying ABF with the aid of adding multiple AEs at each of the TAAs and the RAAs at the transmitter and receiver. Note that the MSF-STSK systems considered in this section were not compared to their equivalent-throughput OFDM-MS-STSK counterparts, since for the considered configurations no equivalent-throughput OFDM-MS-STSK systems can be employed.

## IV. CONCLUSIONS

In this paper we proposed a novel OFDM-MS-STSK system for communications over mmWaves, which strikes a flexible trade-off between the attainable throughput and the achievable diversity gain. This system sub-divides the overall bandwidth into a high number of sub-carriers, where a single STSK codeword is transmitted over each sub-carrier by implicitly carrying the activated AC index. Furthermore, for the sake of mitigating the effect of the high path loss, ABF is employed in conjunction with a pair of phase-shifters and power amplifiers connected to each antenna element, where each antenna array contains multiple antenna elements at both the transmitter and receiver. Furthermore, the OFDM-MS-STSK system was extended to invoke the frequency domain for further enhancing the transmission rate with the aid of frequency indexing in the MSF-STSK system. Due to the large bandwidths available at mmWaves, a high number of sub-carriers can be used for OFDM systems, which can be subdivided into blocks in

order to spread the transmit information both over space-time and frequency. The MSF-STSK system is capable of further enhancing the multiplexing gain of the system at the cost of an increased complexity. However, for the sake of reducing the overall detection complexity order, HL-ML was employed for both the OFDM-MS-STSK and MSF-STSK schemes.

## REFERENCES

- [1] T. Rappaport, S. Sun, R. Mayzus, H. Zhao, Y. Azar, K. Wang, G. Wong, J. Schulz, M. Samimi, and F. Gutierrez, "Millimeter Wave Mobile Communications for 5G Cellular: It Will Work!" *IEEE Access*, vol. 1, pp. 335–349, 2013.
- [2] Z. Pi and F. Khan, "An Introduction to Millimeter-Wave Mobile Broadband Systems," *IEEE Communications Magazine*, vol. 49, no. 6, pp. 101–107, June 2011.
- [3] S. Hur, S. Baek, B. Kim, Y. Chang, A. F. Molisch, T. S. Rappaport, K. Haneda, and J. Park, "Proposal on Millimeter-Wave Channel Modeling for 5G Cellular System," *IEEE Journal of Selected Topics in Signal Processing*, vol. 10, no. 3, pp. 454–469, April 2016.
- [4] G. R. Maccartney, T. S. Rappaport, M. K. Samimi, and S. Sun, "Millimeter-Wave Omnidirectional Path Loss Data for Small Cell 5G Channel Modeling," *IEEE Access*, vol. 3, pp. 1573–1580, 2015.
- [5] S. Hur, T. Kim, D. Love, J. Krogmeier, T. Thomas, and A. Ghosh, "Millimeter Wave Beamforming for Wireless Backhaul and Access in Small Cell Networks," *IEEE Transactions on Communications*, vol. 61, no. 10, pp. 4391–4403, October 2013.
- [6] L. Hanzo, M. El-Hajjar, and O. Alamri, "Near-Capacity Wireless Transceivers and Cooperative Communications in the MIMO Era: Evolution of Standards, Waveform Design, and Future Perspectives," *Proceedings of the IEEE*, vol. 99, no. 8, pp. 1343–1385, Aug 2011.
- [7] P. Wolniansky, G. Foschini, G. Golden, and R. Valenzuela, "V-BLAST: An Architecture for Realizing Very High Data Rates Over The Rich-Scattering Wireless Channel," in *International Symposium on Signals, Systems, and Electronics (ISSSE)*, Sep 1998, pp. 295–300.
- [8] S. Alamouti, "A Simple Transmit Diversity Technique for Wireless Communications," *IEEE Journal on Selected Areas in Communications*, vol. 16, no. 8, pp. 1451–1458, Oct 1998.
- [9] V. Tarokh, H. Jafarkhani, and A. Calderbank, "Space-Time Block Codes From Orthogonal Designs," *IEEE Transactions on Information Theory*, vol. 45, no. 5, pp. 1456–1467, Jul 1999.
- [10] L. Hanzo, T. Liew, B. Yeap, R. Tee, and S. Ng, *Turbo Coding, Turbo Equalisation and Space-Time Coding: EXIT-Chart-Aided Near-Capacity Designs for Wireless Channels*. Wiley, 2011. [Online]. Available: <https://books.google.co.uk/books?id=i0gRC0wGVfGc>
- [11] R. Mesleh, H. Haas, S. Sinanovic, C. W. Ahn, and S. Yun, "Spatial Modulation," *IEEE Transactions on Vehicular Technology*, vol. 57, no. 4, pp. 2228–2241, July 2008.
- [12] P. Yang, M. D. Renzo, Y. Xiao, S. Li, and L. Hanzo, "Design Guidelines for Spatial Modulation," *IEEE Communications Surveys and Tutorials*, vol. 17, no. 1, pp. 6–26, First Quarter 2015.
- [13] P. Yang, Y. Xiao, Y. L. Guan, K. V. S. Hari, A. Chockalingam, S. Sugiura, H. Haas, M. D. Renzo, C. Masouros, Z. Liu, L. Xiao, S. Li, and L. Hanzo, "Single-Carrier SM-MIMO: A Promising Design for Broadband Large-Scale Antenna Systems," *IEEE Communications Surveys Tutorials*, vol. 18, no. 3, pp. 1687–1716, thirdquarter 2016.
- [14] P. Liu and A. Springer, "Space Shift Keying for LOS Communication at mmWave Frequencies," *IEEE Wireless Communications Letters*, vol. 4, no. 2, pp. 121–124, April 2015.
- [15] L. L. Hanzo, O. Alamri, M. El-Hajjar, and N. Wu, *Near-Capacity Multi-Functional MIMO Systems: Sphere-Packing, Iterative Detection and Cooperation*, ser. IEEE. Wiley, 2009. [Online]. Available: <http://books.google.co.uk/books?id=590-JItOJREC>
- [16] M. El-Hajjar, O. Alamri, J. Wang, S. Zummo, and L. Hanzo, "Layered Steered Space-Time Codes Using Multi-Dimensional Sphere Packing Modulation," *IEEE Transactions on Wireless Communications*, vol. 8, no. 7, pp. 3335–3340, July 2009.
- [17] S. Sugiura, S. Chen, and L. Hanzo, "Space-Time Shift Keying: A Unified MIMO Architecture," in *IEEE Global Telecommunications Conference*, Dec 2010, pp. 1–5.
- [18] I. A. Hemadeh, M. El-Hajjar, S. Won, and L. Hanzo, "Multi-Set Space-Time Shift-Keying With Reduced Detection Complexity," *IEEE Access*, vol. 4, pp. 4234–4246, 2016.
- [19] —, "Layered Multi-Group Steered Space-Time Shift-Keying for Millimeter-Wave Communications," *IEEE Access*, vol. 4, pp. 3708–3718, 2016.
- [20] S. Sun, T. Rappaport, R. Heath, A. Nix, and S. Rangan, "MIMO for Millimeter-Wave Wireless Communications: Beamforming, Spatial Multiplexing, or Both?" *Communications Magazine, IEEE*, vol. 52, no. 12, pp. 110–121, December 2014.
- [21] O. El Ayach, S. Rajagopal, S. Abu-Surra, Z. Pi, and R. Heath, "Spatially Sparse Precoding in Millimeter Wave MIMO Systems," *IEEE Transactions on Wireless Communications*, vol. 13, no. 3, pp. 1499–1513, March 2014.
- [22] S. Kutty and D. Sen, "Beamforming for Millimeter Wave Communications: An Inclusive Survey," *IEEE Communications Surveys Tutorials*, vol. 18, no. 2, pp. 949–973, Secondquarter 2016.
- [23] T. Rappaport, J. Murdock, and F. Gutierrez, "State of the Art in 60-GHz Integrated Circuits and Systems for Wireless Communications," *Proceedings of the IEEE*, vol. 99, no. 8, pp. 1390–1436, Aug 2011.
- [24] S. Sugiura and L. Hanzo, "Single-RF Spatial Modulation Requires Single-Carrier Transmission: Frequency-Domain Turbo Equalization for Dispersive Channels," *IEEE Transactions on Vehicular Technology*, vol. 64, no. 10, pp. 4870–4875, Oct 2015.
- [25] E. Basar, U. Aygolu, E. Panayirci, and H. V. Poor, "Orthogonal Frequency Division Multiplexing With Index Modulation," *IEEE Transactions on Signal Processing*, vol. 61, no. 22, pp. 5536–5549, Nov 2013.
- [26] M. Wen, X. Cheng, M. Ma, B. Jiao, and H. V. Poor, "On the Achievable Rate of OFDM With Index Modulation," *IEEE Transactions on Signal Processing*, vol. 64, no. 8, pp. 1919–1932, April 2016.
- [27] B. Zheng, F. Chen, M. Wen, F. Ji, H. Yu, and Y. Liu, "Low-Complexity ML Detector and Performance Analysis for OFDM With In-Phase/Quadrature Index Modulation," *IEEE Communications Letters*, vol. 19, no. 11, pp. 1893–1896, Nov 2015.
- [28] N. Ishikawa, S. Sugiura, and L. Hanzo, "Subcarrier-Index Modulation Aided OFDM - Will It Work?" *IEEE Access*, vol. 4, pp. 2580–2593, 2016.
- [29] H. Zhang, L. L. Yang, and L. Hanzo, "Compressed Sensing Improves the Performance of Subcarrier Index-Modulation-Assisted OFDM," *IEEE Access*, vol. 4, pp. 7859–7873, 2016.
- [30] T. Datta, H. S. Eshwarajah, and A. Chockalingam, "Generalized Space-and-Frequency Index Modulation," *IEEE Transactions on Vehicular Technology*, vol. 65, no. 7, pp. 4911–4924, July 2016.
- [31] H. A. Ngo, C. Xu, S. Sugiura, and L. Hanzo, "Space-Time-Frequency Shift Keying for Dispersive Channels," *IEEE Signal Processing Letters*, vol. 18, no. 3, pp. 177–180, March 2011.
- [32] M. Kadir, S. Sugiura, S. Chen, and L. Hanzo, "Unified MIMO-Multicarrier Designs: A Space-Time Shift Keying Approach," *Communications Surveys Tutorials, IEEE*, vol. 17, no. 2, pp. 550–579, Secondquarter 2015.
- [33] S. Sugiura, S. Chen, and L. Hanzo, "Coherent and Differential Space-Time Shift Keying: A Dispersion Matrix Approach," *IEEE Transactions on Communications*, vol. 58, no. 11, pp. 3219–3230, November 2010.
- [34] M. Samimi and T. Rappaport, "Ultra-Wideband Statistical Channel Model for Non Line of Sight Millimeter-Wave Urban Channels," in *Global Communications Conference (GLOBECOM)*, IEEE, Dec 2014, pp. 3483–3489.
- [35] T. Rappaport, G. Maccartney, M. Samimi, and S. Sun, "Wideband Millimeter-Wave Propagation Measurements and Channel Models for Future Wireless Communication System Design," *IEEE Transactions on Communications*, vol. 63, no. 9, pp. 3029–3056, Sept 2015.
- [36] H. Xu, T. Rappaport, R. Boyle, and J. Schaffner, "Measurements And Models for 38-GHz Point-to-Multipoint Radiowave Propagation," *IEEE Journal on Selected Areas in Communications*, vol. 18, no. 3, pp. 310–321, March 2000.
- [37] B. Razavi, "A 60-GHz CMOS Receiver Front-End," *IEEE Journal of Solid-State Circuits*, vol. 41, no. 1, pp. 17–22, Jan 2006.
- [38] M. C. Lee, W. H. Chung, and T. S. Lee, "Generalized Precoder Design Formulation and Iterative Algorithm for Spatial Modulation in MIMO Systems With CSIT," *IEEE Transactions on Communications*, vol. 63, no. 4, pp. 1230–1244, April 2015.
- [39] M. K. Samimi and T. S. Rappaport, "3-D Statistical Channel Model For Millimeter-Wave Outdoor Mobile Broadband Communications," in *International Conference on Communications (ICC)*, IEEE, June 2015, pp. 2430–2436.
- [40] —, "Local Multipath Model Parameters for Generating 5G Millimeter-Wave 3GPP-Like Channel Impulse Response," in *10th European Conference on Antennas and Propagation (EuCAP)*, April 2016, pp. 1–5.

- [41] A. Maltsev, V. Erceg, E. Perahia, C. Hansen, R. Maslennikov, A. Lomayev, A. Sevastyanov, A. Khoryaev, G. Morozov, M. Jacob, S. Priebe, T. K  ijrner, S. Kato, H. S. mand Katsuyoshi Sato, and H. Harada, "Channel Models for 60 GHz WLAN Systems," pp. c1–187, May 2010. [Online]. Available: [http://www.ieee802.org/11/Reports/tgad\\_update.htm](http://www.ieee802.org/11/Reports/tgad_update.htm)
- [42] IEEE, "IEEE WPAN 802.15.3c Millimeter-Wave based Alternative Physical Layer Extension," pp. c1–187, Oct 2009. [Online]. Available: <http://www.ieee802.org/15/pub/TG3c.html>
- [43] G. Maccartney, T. Rappaport, S. Sun, and S. Deng, "Indoor Office Wideband Millimeter-Wave Propagation Measurements and Channel Models at 28 and 73 GHz for Ultra-Dense 5G Wireless Networks," *Access, IEEE*, vol. 3, pp. 2388–2424, 2015.
- [44] T. S. Rappaport, G. R. MacCartney, M. K. Samimi, and S. Sun, "Wideband Millimeter-Wave Propagation Measurements and Channel Models for Future Wireless Communication System Design," *IEEE Transactions on Communications*, vol. 63, no. 9, pp. 3029–3056, Sept 2015.
- [45] M. Driusso, F. Babich, M. Kadir, and L. Hanzo, "OFDM Aided Space-Time Shift Keying for Dispersive Downlink Channels," in *Vehicular Technology Conference (VTC Fall)*, IEEE, Sept 2012, pp. 1–5.
- [46] M. Kadir, S. Sugiura, J. Zhang, S. Chen, and L. Hanzo, "OFDMA/SC-FDMA Aided Space-Time Shift Keying for Dispersive Multiuser Scenarios," *IEEE Transactions on Vehicular Technology*, vol. 62, no. 1, pp. 408–414, Jan 2013.
- [47] M. Kadir, S. Chen, and L. Hanzo, "A Reduced-Complexity Detector for OFDMA/SC-FDMA-Aided Space-Time Shift Keying," in *Vehicular Technology Conference (VTC Fall)*, 2013 IEEE 78th, Sept 2013, pp. 1–5.



**SeungHwan Won** (M'04) received the B.S. and M.S. degrees in Radio Science and Engineering from Korea University, Seoul, Republic of Korea, in 1999 and 2001, respectively. He was a research engineer in Mobile Communication Technology Research Lab, LG Electronics R&D, from January 2001 to September 2004. He was the recipient of the 2004 state scholarship of the Information and Telecommunication National Scholarship Program, Ministry of Information and Communication (MIC), Republic of Korea. During 2004 and 2008 he conducted research, working towards the Ph.D. degree in the Communications Research Group, School of Electronics and Computer Science at the University of Southampton, UK. His major research interests included initial synchronization in non-coherent MIMO aided single- and multi-carrier CDMA, IDMA and OFDMA as well as in iterative synchronization schemes designed for MIMO aided single- and multi-carrier transmission systems. He published a host of papers in these research fields. Upon completing his PhD he returned to his native Korea and joined Samsung. In 2013 he was appointed as an Associate Prof. by the University of Southampton and currently he is teaching and conducting research at the campus of the University of Southampton in Johor, Malaysia.



Multi-user MIMO.

**Ibrahim Hemadeh** received his BEng degree (with first class honour) in Computer and Communications Engineering from the Islamic University of Lebanon in 2010. He then received an MSc in Wireless Communications (with distinction) from the University of Southampton, UK in 2012. He is currently pursuing his PhD in Wireless Communications with the University of Southampton under the supervision of Prof Lajos Hanzo and Dr Mohammed El-Hajjar. His research interests mainly include millimeter wave communications, Multi-functional MIMO and



**Lajos Hanzo** received the master's degree in electronics, the Ph.D. degree, and the Doctor Honoris Causa degree from the Technical University of Budapest, in 1976, 1983, and 2009, respectively, and the Doctor Honoris Causa degree from the University of Edinburgh in 2015. During his 40-year career in telecommunications, he has held various research and academic positions in Hungary, Germany, and the U.K. Since 1986, he has been with the School of Electronics and Computer Science, University of Southampton, U.K., as the Chair in Telecommunica-

tions. He has successfully supervised 110 Ph.D. students, co-authored 20 John Wiley/IEEE Press books in mobile radio communications totaling in excess of 10 000 pages, co-authored over 1 600 research contributions found at the IEEE Xplore, acted as the TPC Chair and General Chair of the IEEE conferences, presented keynote lectures, and received a number of distinctions. He is directing a 60 strong academic research team, involved in a range of research projects in the field of wireless multimedia communications sponsored by the industry, the Engineering and Physical Sciences Research Council, U.K., the European Research Councils Advanced Fellow Grant, and the Royal Societies Wolfson Research Merit Award. He is an enthusiastic supporter of industrial and academic liaison and offers a range of industrial courses. He is also a fellow of the Royal Academy of Engineering, the Institution of Engineering and Technology, and the European Association for Signal Processing. He is a Governor of the IEEE ComSoc and of VTS. From 2008 to 2012, he was the Editor-in-Chief of the IEEE Press and a Chaired Professor with Tsinghua University, Beijing. He has 25 000+ citations.



**Mohammed El-Hajjar** is a lecturer in the Electronics and Computer Science in the University of Southampton. He received his BEng degree in Electrical Engineering from the American University of Beirut, Lebanon in 2004. He then received an MSc in Radio Frequency Communication Systems and PhD in Wireless Communications both from the University of Southampton, UK in 2005 and 2008, respectively. Following the PhD, he joined Imagination Technologies as a design engineer, where he worked on designing and developing Imagination's

multi-standard communications platform, which resulted in three patents. In January 2012, he joined the Electronics and Computer Science in the University of Southampton as a lecturer in the Southampton Wireless research group. He is the recipient of several academic awards including the Dean's award for creative achievement, Dorothy Hodgkin postgraduate award and IEEE ICC 2010 Best paper award. He has published a Wiley-IEEE book and in excess of 60 journal and international conference papers. His research interests are mainly in the development of intelligent communications systems including energy-efficient transceiver design, MIMO, millimetre wave communications and Radio over fibre systems.